Instability Mode Interaction in a Spacially Developing Plane Wake

AUTHOR(S):

Maekawa, Hiroshi; Mansour, Nagi N.; Buell, Jefferey C.

CITATION:

Maekawa, Hiroshi ...[et al]. Instability Mode Interaction in a Spacially Developing Plane Wake. 数理解析研究所講究録 1990, 719: 11-47

ISSUE DATE:

1990-05

URL:

http://hdl.handle.net/2433/101811

数理解析研究所講究録
719巻 1990年 11-47

Instability Mode Interaction in a Spacially Developing Plane Wake

Kagoshima University, Hiroshi Maekawa (前川博)
NASA Ames Research Center, Nagi N. Mansour
NASA Ames Research Center, Jefferey C. Buell

The transition mechanism in a two-dimensional wake was studied by means of direct numerical simulations of a spatially developing wake. The incompressible time-dependent 2-D Navier-Stokes equations were solved using finite difference method in the streamwise direction, pseudospectral Fourier method in the cross-stream direction, and a third order compact Runge-Kutta scheme for time advancement. The unstable eigenfunctions of the Orr-Sommerfelt equations were used to perturb a Gaussian wake of the inlet plane; only fundamental mode, fundamental and two subharmonics, fundamental mode and random phase noise, and only random phase noise. The wake flows forced with the eigenfunctions of small and considerable amplitudes were investigated.

The statistical analysis was performed and some numerical results were compared with the experimental measurements. When only the fundamental mode is introduced, whose amplitude is large of 0.01 of free stream velocity, the energy spectra show the generation of harmonics. Unperturbed alternate vortices are generated in the downstream. While the inlet plane is forced by the fundamental mode and two subharmonics; numerical results show the harmonics components of 2nd subharmonic. The alternate vortices are purturbed the downstream. The selective

amplification of a few modes around the fundamental mode is observed in case of random phase noise of large amplitude. The irregular fluctuation of phase around the fundamental mode play a critical role to generating vortices at different downstream locations. Therefore, the large and small-scale distortions of vortical structure are observed in the further downstream. The velocity signals in the further downstream show growth of irregular component. The energy spectra of low-frequency component become larger than that of the fundamental mode in the further downstream. The strong interaction among some of same and opposite sign vortices was observed, in which process a pairing motion of same sign vortives and some couple vortices of different signs are generated.

When the amplitude of fluctuation at the inlet plane is zero in the computation, the wake becomes laminar even at Reynolds number 600. While the inlet plane is forced by the random phase noise of the amplitude of 0.00001 of free stream velocity, the fundamental mode selectively grows faster than other modes. The spectra show a sharp peak at the fundamental mode. When the amplitudes of the fundamental mode and two subharmonics at the inlet plane are 0.00001, a random motion is created in the flow, so that the spectra have continuous components, as well as the fundamental mode.

In case of a very large-deficit wake, the flow is absolutely unstable at Reynolds number 700, no forcing after short time disturbance makes the alternate vortices downstream. The fluctuation sustains in the upstream during no forcing.

1. Introduction

The study of laminar-turbulent transition in a plane wake, as well as jet flow and separated flow, has been fundamental and very important to the understanding of the mechanism of transition of free boundary shear flow. In two decades, non-linear and randomizing regions of the transition in a plane wake have been investigated by numerical and experimental works.

The experimental studies of the wake have been carried out extensively by Sato et. al. (1961), (1970), (1975), (1978) and Mattignly & Criminale (1972). Ditailed measurements were made on the laminar-turbulent transition of two-dimensional wake with many kinds of imposed disturbances; natural disturbance in a wind tunnel, a sound of single frequency, a sound of two frequency from outside and etc.. In all cases the transition to turbulence was gradual.

Sato & Onda (1970) repoted that when the artificial disturbance was introduced, the transition took place in different manner. The whole transition process strongly depends on the initial disturbance. In non-linear region, They repoted the generation of velocity fluctuations of subtraction and addition of two artificial frequencies. They conjectured that the slow and irregular fluctuation found in the natural transition might be ganerated by the same process of the subtraction of two artificial frequencies. They explained the experimental results by two empirical properties of the nonlinear interaction: the growth suppression induced by a large amplitude fluctuation and the stronger interaction between fluctuations of closer amplitudes.

On the other hand, Zabusky and Deem (1971) calculated time developing wakes with a single exited eigenmode for the initial condition using a finite-difference method and showed the existence of a double row of elliptical vortices. They showed first harmonic energy profiles with off-axis nulls, and second harmonics phase profiles of the cross-stream direction, which was similar to the measurements. Numerical simulations have focused on the longitudinal spatial spectral statistics. Transverse (cross-stream) averages of the longitudinal energies showed the approximate power law $E_k \sim k^{-n}$, where $3 \leq n \leq 4$. Hannemann (1987) simulated absolutely and convectively unstable regions behind a flat plate with a thick trailing edge using a finite difference method. The temporal amplification process of perturbations at supercritical Reynolds numbers was studied. Hultgren & Aggarwal (1987) showed the critical defect value and supercritical Reynolds numbers of absolutely unstable Gaussian wakes by non-linear stability theory.

However, There is still a large gap between the understanding about nonlinear interaction and randomization by numerical simulations and that by laboratory measurements. It is difficult for the numerical simulation of time developing transition flow to present the whole spatially evolution process of statistics measured by the experiments. While the experiment measurement is usually hard to offer the time dependent structual evolution such as vorticity and pressure.

The purpose of this investigation is to presnt the spatially evoluting process of various instability modes interaction and the flow dynamics that are crucial to the understanding of the

evolving structure which governs the transition flow. The non-linear region and the beginning of randomness are studied by means of the statistical analysis of deterministic and random components created in the flow with various disturbances; for example, linear instability modes and random phase noise. The effect of interaction of these modes on the flow structure is systematically investigated. Moreover, a very large-deficit Gaussian wake is studied from the view of an absolute unstable motion. This paper tries to understand the transition mechanism determined with the experimental measurement.

2. Mathematical formulation

2.1 governing field equations

Computational domain starts downstream of the trailing-edge of a spliter plate. Figure 1 illustrates computational set up and the coordinate system used. The x-axis represents the streamwise flow direction. The y-axis represents the cross-stream direction perpendicular to x. The streamwise extent of the computational domain is finite and the y extent is infinite in both the positive and negative y directions. The time-dependent incompressible Navier-Stokes equations are

$$\frac{\partial u_i}{\partial t} = \epsilon_{ijk} u_j \omega_k - \frac{\partial P}{\partial x_i} + Re^{-1} \nabla^2 u_i \qquad (1)$$

where P is the dynamic pressure and $Re = U b_{\frac{1}{2}} / \nu$, $b_{\frac{1}{2}}$ represents the half width of the inlet laminar wake flow. The conservation of mass for the fluid is expressed by the continuity equation:

$$\frac{\partial u_i}{\partial x_i} = 0. \tag{2}$$

All quantities are non-dimensionalized by the appropriate characteristic scales, U and $b_{\frac{1}{2}}$.

2.2 Boundary conditions

A Gaussian profile was chosen for an inlet flow condition, namely, the mean u component of velocity at the inlet plane is represented by:

$$u = 1 - 0.692 \exp(-0.69315 y^2) \tag{3}$$

The coefficient 0.692 in equation (3) is used so that the center-line deficit will correspond to the experiment by Sato & Kuriki (1961). In the study of large-deficit wake, this coefficient is set at 0.99. The other coefficient 0.69315 is set so that the half-width of the profile is 1 at y=1. In addition to the mean flow, the inlet is forced with the eigenfunction perturbations. The unstable eigenfunctions of Rayleigh equation for the Gaussian profile of the equation (3) were calculated. The fundamental mode, first and second subfarmonics are superimposed on the velocity at the inlet plane. These perturbations are of the form

$$u_j^p(y,t) = \frac{1}{2}[\tilde{u}_j(y) e^{i\omega_p t} + C.C.] \tag{4}$$

where ω_p represents the frequency of oscillation of the eigenfunction. The random phase noise is created by the perturbation

$$u_j^{rp}(y,t) = \frac{1}{2}[\hat{u}_j(y) e^{i\omega_{rp} t} + C.C.] \tag{5}$$

where ω_{rp} is the random frequency generated by a random function. In this work, only the v component was used for the perturbation.

A time dependent advection condition of the form:

$$\frac{\partial u_i}{\partial t} + U_a \frac{\partial u_i}{\partial x} = 0 \tag{6}$$

in invoked for each of the velocity components at the exit plane, where U_a represents the advection speed of the large-scale structures in the layer. This approarch has been taken in other simulations of spatially developing free shear layers (see Davis & Moore (1985)). The choise of U_a=U is appropriate for the simulation of the small-deficit wake at the exit plane. We use a large computational domain in x direction, so that the exit plane is small-deficit wake.

The velocity components are splitted into computational variables and "reference" profiles. Specially,

$$\begin{aligned} u &= u_c + U(y) \\ v &= v_c \end{aligned} \tag{7}$$

where the computational variable are denoted by subscript c. Boundary conditions at infinity are that all fluctuations and their derivatives are zero. The mapping (Cain et al. 1984) employed in this work moved the points at infinity into computable range.

2.3 Initial conditions

The Gaussian profile prescribed for the mean u component at the inlet plane is distributed uniformly at all x locations in the domain at t=0. This profile is perturbed with eigenfunctions,

but only at the inlet plane. These initial conditions must be allowed to wash out before any statistical analysis may be performed on the layer. Laminar flow profiles calculated with no forcing at the inlet plane are used as the initial condition to simulate the large-deficit wake.

3. Numerical method

The two-dimensional Navier-Stokes equations are solved on a domain that is infinite in the y dirrection and finite in the x direction. Pressure is eliminated by taking the curl of equation (1) twice. This yields a forth-order equation for the streamwise velocity u as follows:

$$\frac{\partial \nabla^2 u}{\partial t} = h + Re^{-1} \nabla^4 u \tag{8}$$

where $$h = -\frac{\partial}{\partial y}\left(\frac{\partial H_1}{\partial y} - \frac{\partial H_2}{\partial x}\right)$$

H_i includes the convective terms.

Equation (8) is advanced in time explicitly using a compact third-order Runge-Kutta scheme by Wray (1980). Since the Laplacian is contained in the time-derivative term, a Poisson equation must be solved during each substep. As in primitive variable algorithms, it is the way in which this Poisson equation is solved that guarantees conservation of mass. The cross-stream velocity v is recovered directly from the continuity equation (2). The algorithm is based on a Fourier method with a cotangent mapping in the y direction, and high-order accurate Padé approximations in the x direction. The first x-derivatives in the

continuity equation and in the advection terms are approximated with modified Padé finite differencing (S. Lele, private communication). The particular approximation used here yields sixth-order accuracy for the low to moderate wavenumber components of the solution, and significantly less dispersion errors for high wavenumbers. The second and fourth-order x-derivatives are approximated with classical Padé formulas. In order to avoid the inversion of very large sparse matrices for the solution of the Poisson equation, the effective wavenumber concept by Kim & Moin (1985) is applied in the x direction. It is implemented by subtracting off certain boundary terms and the expanding the solution in a sineseries. A sine transformation decouples the modes and allows the solution to be obtained by aseries of one-dimensional inversion of the y direction approximation. The algorithm contains no numerical diffusion, which we believe is important for problems where the dynamics is important, and which contain many regions of strong gradients. Furthermore, without numerical diffusion, marginal resolution will usually appear as high-wavenumber oscillations and is thus easily detected. Details and numerical analytic tests of the scheme will be presented elsewhere.

4. Vortical structure in a plane wake

4.1 Present numerical simulations

Five cases were studied in the present work: The first (Case 1) is a wake flow forced with a fundamental mode only. The second (Case 2) is a wake flow forced by the fundamental mode and its first subharmonic. The third one (Case 3) is forced by the

fundamental mode and its first and second subharmonics, whose phase rag is zero dgree. The fourth one (Case 4) is forced by the fundamental mode and a random phase noise. In this case, the amplitudes of the fundamental mode and random phase noise are 0.01 and 0.0005 of free stream U velocity respectively. The fifth one (Case 5) is forced with the random phase noise only. In Cases 1 and 2, the amplitudes of purturbation were 0.01. In Cases 3 and 5, the amplitudes were 0.0, 0.00001 and 0.01 of free stream U velocity. The Reynolds number, which based on the half-value width at the inlet plane, ranged from 200 to 700. In the x direction ($0 \leq x \leq 200$) at Re=200, 384 uniformly distributed grid points were used and 64 grid points in the y direction. At Re=300, 512 grid points were used in the x direction ($0 \leq x \leq 200$) and 128 grid points in the y direction. At Re=600, 768 grid points were used in the x direction ($0 \leq x \leq 200$), 1536 grid points in the x direction ($0 \leq x \leq 400$), and 128 grid points in the y direction. In case of the very large deficit wake, 1536 grid points were used in the x direction ($0 \leq x \leq 300$) and 128 grid points in the y direction. The inlet plane was forced by the fundamental mode of the amplitude 0.0001 for only one period.

4.2 Generation of vortical structure

Flow visualization of numerical results show the generation of vortex street downstream. In Case 1, the unperturbed vortex street can be observed as shown in Fig. 2. The time traces of velocities are periodic. The spectra have fundamental and its higher harmonics can be seen. In Case 3, in which the amplitude of the purturbation is 0.01, the vortex street is perturbed in the downstrem location. The time traces of velocities are still

periodic but different from those of Case 1. The spectra show the higher harmonics of the second subharmonics. Vorticity contours show the deformation of vortex street in the downstream. Figure 3 shows the vorticity contour of Case 3. In Case 5, the amplitude is 0.00001, the vortex street is deformed. The deformation is gradual in the downstream. The energy spectra have a sharp peak of the fundamental mode and a lot of continuous components. In Case 5, the amplitude is 0.01, the vortical structure becomes chaotic, as shown in Fig.4. The strong interaction between a vortex close to the wake center and the other vortices makes a large-scale deformation. This deformation is observed to be a well organized motion, where a pairing of vortices and vortex couples are found in the further downstream.

4.2.1 Time evolving strong interaction

In this subsection, we observe the time evolving process of vortex pairing. Pairing phenomena have never seen in a plane wake by experimental measurements (Robert & Roshko (1985)). The observation of vorticity contours offer an identification of pairing motion. Figure 5 (a), (b), (c), (d), (e) and (f) show the time evolving vortex dynamics. The plus and minus sign vortices shown as 1, 2, 3, 4 and 5 in Fug.5 (a) change their distances in the downstream locations. Figures 5 (b) and (c) show that the plus sign vortices of 2 and 3, furthermore the minus sign vortices of 3 and 4 start to amalugamate and the vortex of 1 is pushed out toward the downstream. Figure 5 (d) shows that the vortices of 4 and 5 finish to amalugamate; while the vortices of 2 and 3 start to amalugamate. In the upstream of these vortices, an amalugamation of two vortices 8 and 9 also starts , as shown

in Fig.5 (e). After the amalgamation of two vortices of 8 and 9, the vortices 7 and 8 become a couple vortices shown in Fig.5 (f), which is reported in the soup film experiments by Couder & Basdevant (1986).

5. Selective growth of the fundamental mode and randomness

5.1 Growth of the fundamental mode and subharmonics

Figures 6 (a) and (b) show the streamwise distribution of the fundamental mode of u for y=2.2 and y=0.0 respectively in Case 1 at Re=200. We notice in Fig.6 (a) that the peak of the fundamental mode is located around x=50, where alternate vortices are generated. In Fig.6 (b), the distribution of 2nd harmonic has a peak around x=50. In Case 3 at Re=200, the distribution of the fundamental mode and subharmonics at y=2.2 and y=0.0 are shown in Fig.7 (a) and (b) respectively. We notice in Fig.7 (a) that the fundamental mode grows faster than two subharmonics and 1st subharmonic grows after saturating of the fundamental mode. We also notice in Fig.7 (b) that the distribution of 1st subharmonics and 2nd harmonics have peaks around x=50, respectively. At the wake center, the energy of 2nd harmonic component is larger than that of the fundamental mode. We notice from the vorticity contours that the growth of the 2nd harmonic component at the wake center is due to the generation of alternate vortices. In Case 5, the amplitude of random phase noise is 0.00001 of free stream U velocity, the fundamental mode selectively grows in the linear region. Figure 8 shows the spectrum of u at x=50 and y=-0.8. The spectrum has the peak at the fundamental mode and continuous components around the

fundamental mode. We also notice that the 2nd harmonic component and continuous components around the 2nd harmonic component grow at x=50.

5.2 Growth of randomness

We introduced the fundamental mode and the random phase noise of small amplitude at the inlet plane. The amplitude of the fundamental mode was 0.01 and that of the random phase noise 0.0005. Figure 9 show the spectrum of the velocity fluctuation of v at x=50 and y=-0.8. Since the energy of the random phase noise at the inlet plane is lower than 10^{-8}, we notice the growth of the continuous components around the fundamental mode in the downstream locations. Figures 10 (a), (b), (c), (d), (e) and (f) show the cross-stream distribution of the fundamental mode and various continuous components at x=150, in which the frequencies are 0.608, 0.704, 0.508, 0.308 and 0.102. The distributions of the fundamental mode are symmetric, as shown in Fig.10 (a). The profile of u^2 has two peak with off-axis null, which is consistent with the measurement by Sato & Kuriki (1961). Figures 10 (b) and (c) show the profiles of the continuous components around the fundamental mode. These shapes are simillar to that of the fundamental mode. While the shapes of the distributions of the low-frequency noise have far differnt from that of the fundamental mode, as shown in Fig. 10 (d) and (e). Growth of these noises are suppresed strongly by the fundamental mode.

In Case 5, the amplitude is 0.00001, the spectra in the upstream locations show the continuous components around the fundamental mode and also the low-frequency components as shown in Fig.8. Figure 11 show the spectrum of the velocity fluctuation

u in the downstream location of x=150 and y=-2.1. The low-frequency components around the 2nd subharmonic mode grow in the downstream locations after the saturation of the growth of the fundamental mode. In Case of 5, the amplitude is 0.01, a few mode around the fundamental mode grow in the upstream locations. Figures 12 show the spectrum of v at x=25, y=-2.7. We can observe that the spectrum has the continuous components around the fundamental mode but not sharp peak at the fundamental mode. Figure 13 show the spectram of u and v at x=175 and y=-1.7. The energy of the low-frequency noise is larger than that of the fundamental mode. Figures 14 (a) and (b) show the phase diagrams at the same x-y locations of Fig. 12 and Fig. 13, respectively. Figure 14 (a) show the regular motion and chaotic motions, while Fig.14 (b) represent much chaotic motion.

6. Absolute unstable wake

We investigate a very large-deficit wake from the view of absolute instability of the Gaussian wake discussed by Hultgren & Aggarwal (1987). They determined the critical defect parameter and supercritical Reynolds number. We used Gaussian large-deficit profile at the inlet plane, whose deficit was 0.99. The fundamental mode of the amplitude 0.0005 was introduced at the inlet plane for only one periode of the oscillation. The introduction of the fundamental mode was stopped and then no forcing at the inlet plane. We investigate the time traces of the oscillation in the upstream, where the mean defects are smaller than the critical defect reported by them. At Re=300, the disturbance does not keep on sustaining at x=2.0,

where the defect of the mean profile is 0.96. Figure 15 (a) shows the time traces of the u and v fluctuations at y=-0.4 and x=2.0. However, at Re=700, the time traces of the fluctuations of u and v at x=1.4 and y=-0.6, where the mean defect is 0.973, shows that the waves of u and v keep on oscillating in the upstream shown in Fig. 15 (b). The initial disturbance propergates to the upstream, as well as to the downstream, and is amplified in the downstream locations. These facts indicate that the Gaussian wake whose defect is larger than 0.973 is absolutely unstable at Reynolds number 700, which support a part of theoretical results of Hultgren & Aggarwal (1987).

7. Conclutions

Numerical solutions have been presented for the large-scale vortex dynamics and the statistical spectra inside forced two-dimensional wakes. Linear stability theory provides information on many of the important features of the wake. The ensuring computational results compare well with the experimental results of Sato et. al. . Numerical results on the transition process indicate following conclutions.

1. When only the fundamental mode of the large amplitude is invoked, the stable alternate vortices are generated. The higher harmonics are created and grow steeply before the genaration of alternate vortices.

2. When the fundamental mode whose energy level is much larger than that of the noise, the fundamental mode grows steeply and suppress the growth og the other modes. The vortex street created in the downstream is still unperturbed.

3. Two subharmonics with the fundamental mode make the vortical structure distorted in the downstream. When the amplitudes of three modes are large, the higher harmonics of the 2nd harmonics are genarated.

4. When the amplitude of the random phase noise is very small such as 0.00001, the fundamental mode is selectively amplified and grow steeply. The cross-stream profle of the fundamental mode is quite simillar to that of Case 1. The noise sround the fundamental mode grows faster than the low-frequency noise. The low-frequency noise grows after the saturation of the fundamental mode. The vortical structures are distorted in the downstream because of the growth of low-frequency noise.

5. When the amplitude of the random phase noise is 0.01, a few modes close to the fundamental mode are amplified and generate low-frequency modes, so that the strong interaction between several vortices is observed in the downstream. In the process of the strong interaction, pairing motion and vortex couple of different sign are observed. The vortical structure becomes chaotic in the further downstream locations.

6. In case of very large-deficit wake such as 0.99 at the inlet plane, the wake flows become absolutely unstable at Re=700. No forcing after the short time disturbance of a small amplitude makes vortex street.

References

Chain, A. B., Ferziger, J. H. & Reynolds, W. C., 1984, J. Comp. Phys. 56, 272-286.

Couder, Y. & Basdevand, C., 1986, J. Fluid Mech. 173, 225-251.

Hannemann, K., 1987, "Numerical simulation and stability analysis of the absolutely and convectively unstable wake", Ph.D. Thesis, Karlsruhe Univ.

Hultgren, L. S. & Aggarwal A. K., 1987, Physics of Fluid.

Kim, J., Moin, P. & Moser, R., 1987, J. Fluid Mech. 177, 133-166.

Kim, J., Moin, P., 1985, J. Comp. Phys. 59, 308-323.

Mattingly, G. E. & Criminalie, W. O., 1972, J. Fluid Mech. 51, 233-272.

Robrt S. A. & Roshko A., 1985, "Effects of periodic forcing mixing in turbulent shear layer and wakes", AIAA-85-0570.

Sato, H. & Kuriki, K., 1961, J. Fluid Mech. 11, 321-352.

Sato, H. & Onda, Y., 1970, Inst. Space & Aero. Sci., Univ. Tokyo, Report 453, 317-377.

Sato, H. & Saito, H., 1975, J. Fluid Mech. 67, 539-559.

Sato, H. & Saito, H., 1978, J. Fluid Mech. 84, 657-672.

Wray, A. A., 1980, "Very low storage time-advancement schemes", NASA Ames Research Center, Moffett Field, CA.

Zabusky, N. J, & Deem, G. S., 1971, J. Fluid Mech. 47, 353-379.

Figure Captions

Fig. 1: Co-ordinate system, with the basic Gaussian profile.

Fig. 2: Vorticity contour of Case 1 at Re=600.

Fig. 3: Vorticity contour of Case 3 at Re=200.

Fig. 4: Vorticity contour of Case 5 of high-amplitude at Re=600.

Fig. 5: Vorticity contour of pairing motion of Case 5 of high-amplitude at Re=600; (a) at time=900, (b) at time=925, (c) at time=950, (d) at time=975, (e) at time=1025 and (f) at time=1075.

Fig.6: Distribution of the fundamental mode, 2nd harmonics, 1st and 2nd subharmonics in the x locations of Case 1 at Re=200; (a) y=2.2 and (b) y=0.

Fig.7: Distribution of the fundamental mode, 2nd harmonics, 1st and 2nd subharmonics in the x locations of Case 3 at Re=200; (a) y=2.2 and (b) y=0.

Fig.8: Energy spectra of u and v for Case 5 of low-amplitude at x=50 and y=-0.8.

Fig.9: Energy spectrum of v for Case 4 at x=50 and y=-0.8.

Fig.10: Cross-stream distribution of the fundamental mode and noises at x=150; (a) fundamental mode, (b) frequency of 0.704, (c) frequency of 0.508, (d) frequency of 0.152 and (e) frequency of 0.102.

Fig.11: Energy spectra of u and v for Case 5 of low-amplitude at x=150 and y=-2.1.

Fig.12: Energy spectra of u and v for Case 5 of high-amplitude at x=25 and y=-2.7.

Fig.13:Energyspectraof u and v for Case 5 of high-amplitudeat x=175 and y=-0.7.

Fig.14: Phase diagrams for Case 5 of high-amplitude;(a) at x=25 and y=-2.7 and (b) at x=175 and y=-1.7.

Fig.15: Time traces of u and v for very large-deficit wake; (a) at x=2.0 and y=-0.4 at Re=300 and (b) at x=2.7 and y=-0.6 at Re=700.

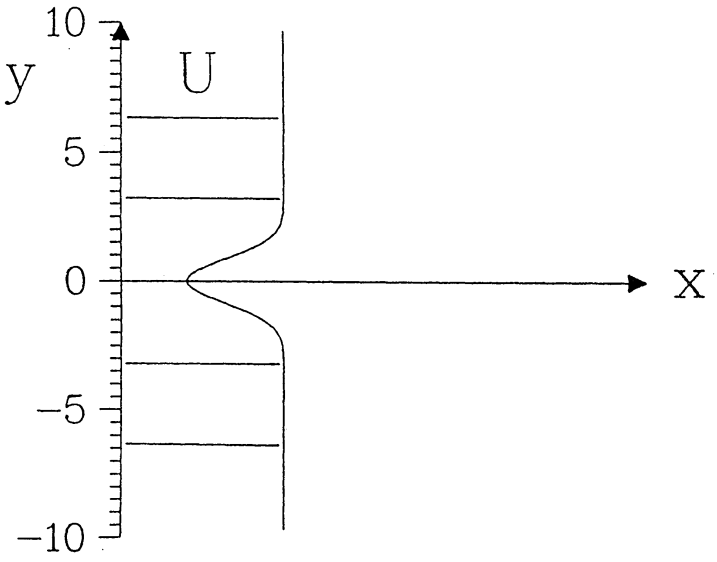

Fig. 1

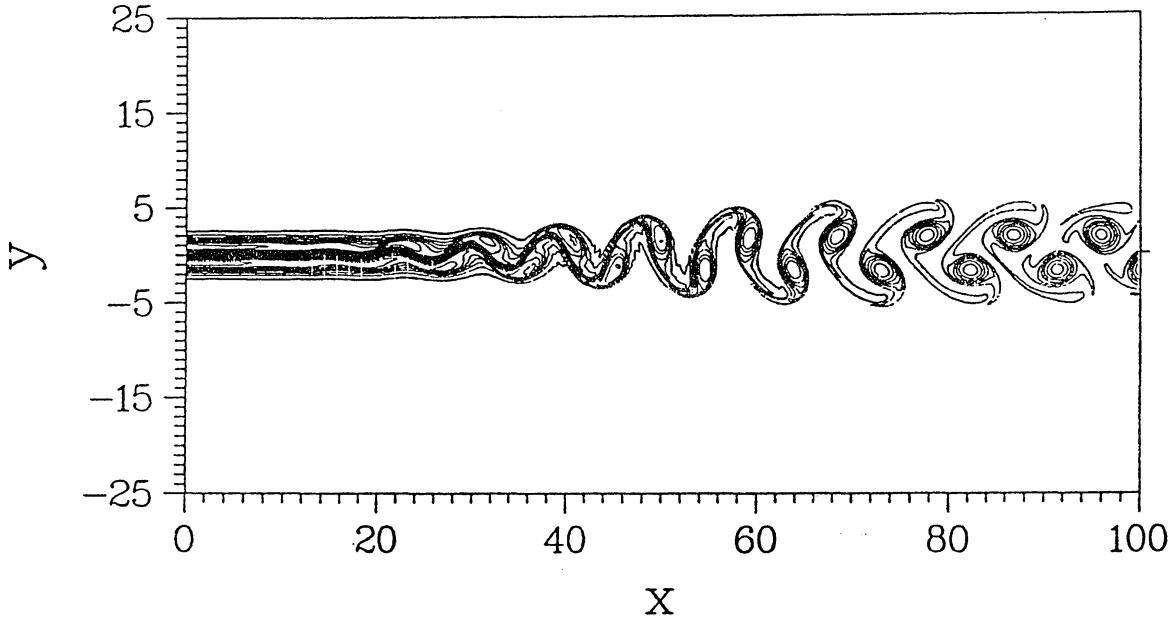
25
15
5
−5
−15
−25
y
0
20
40
60
80
100
X

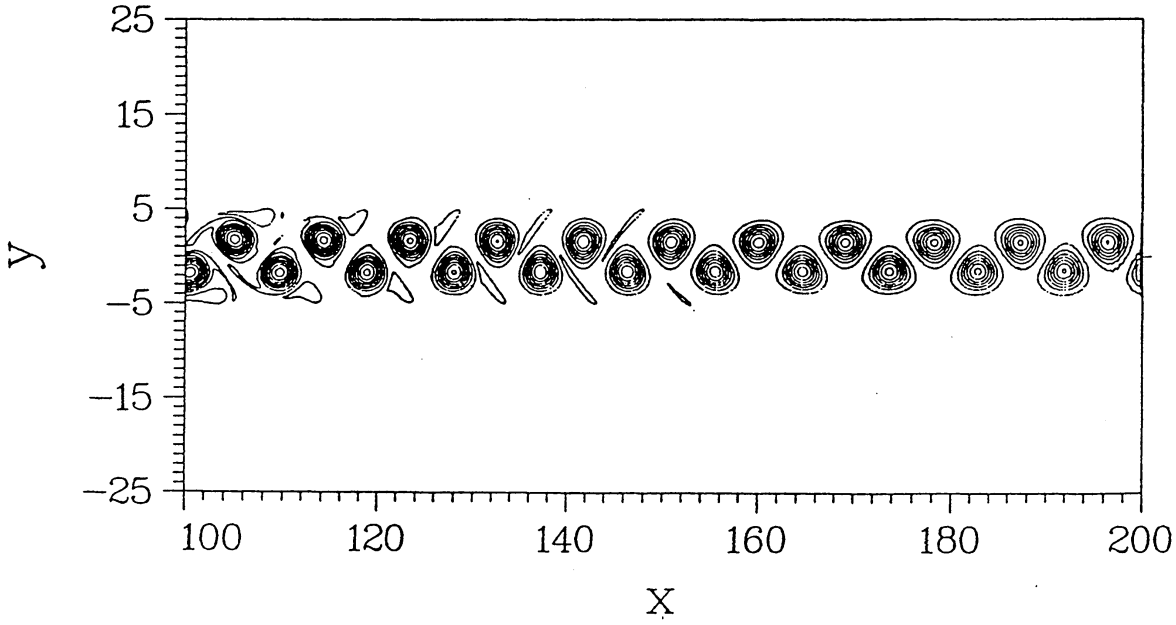
25
15
5
−5
−15
−25
y
100
120
140
160
180
200
X

Fig. 2

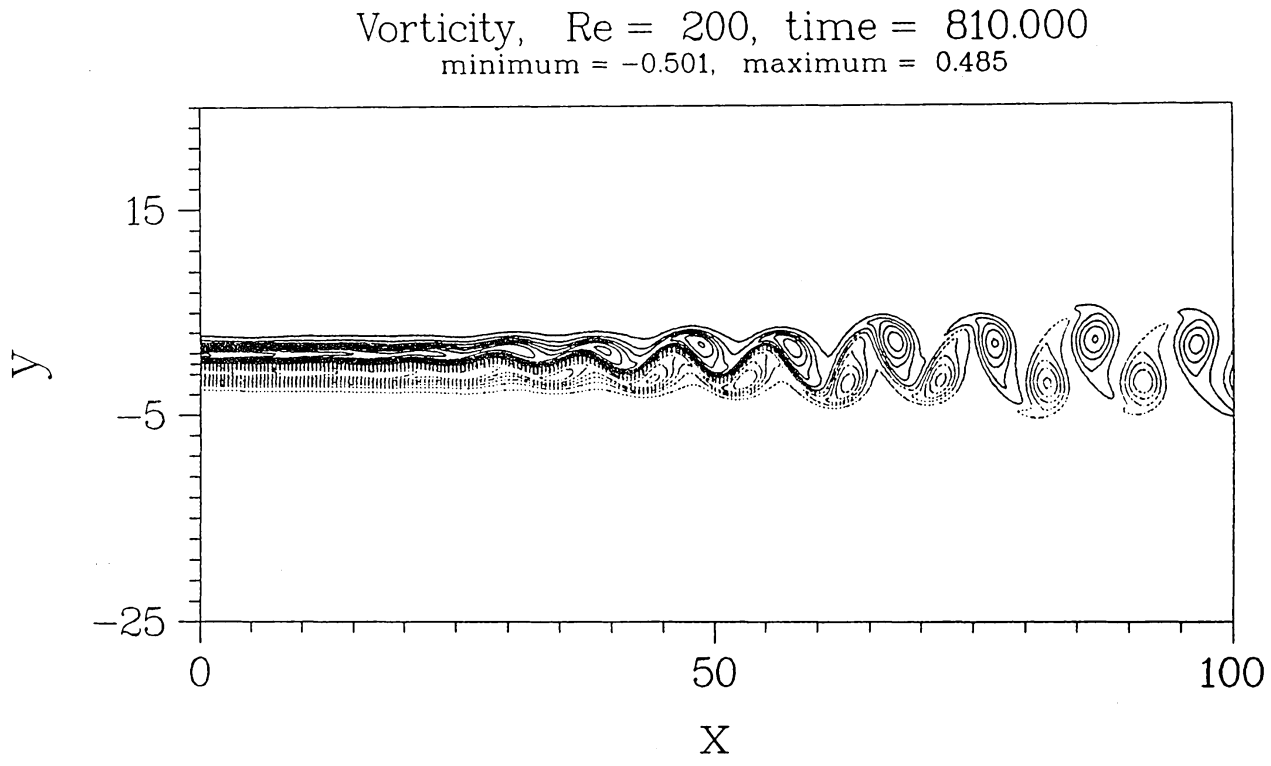
Vorticity, Re = 200, time = 810.000
minimum = −0.501, maximum = 0.485
15
−5
−25
y
0
50
100
X

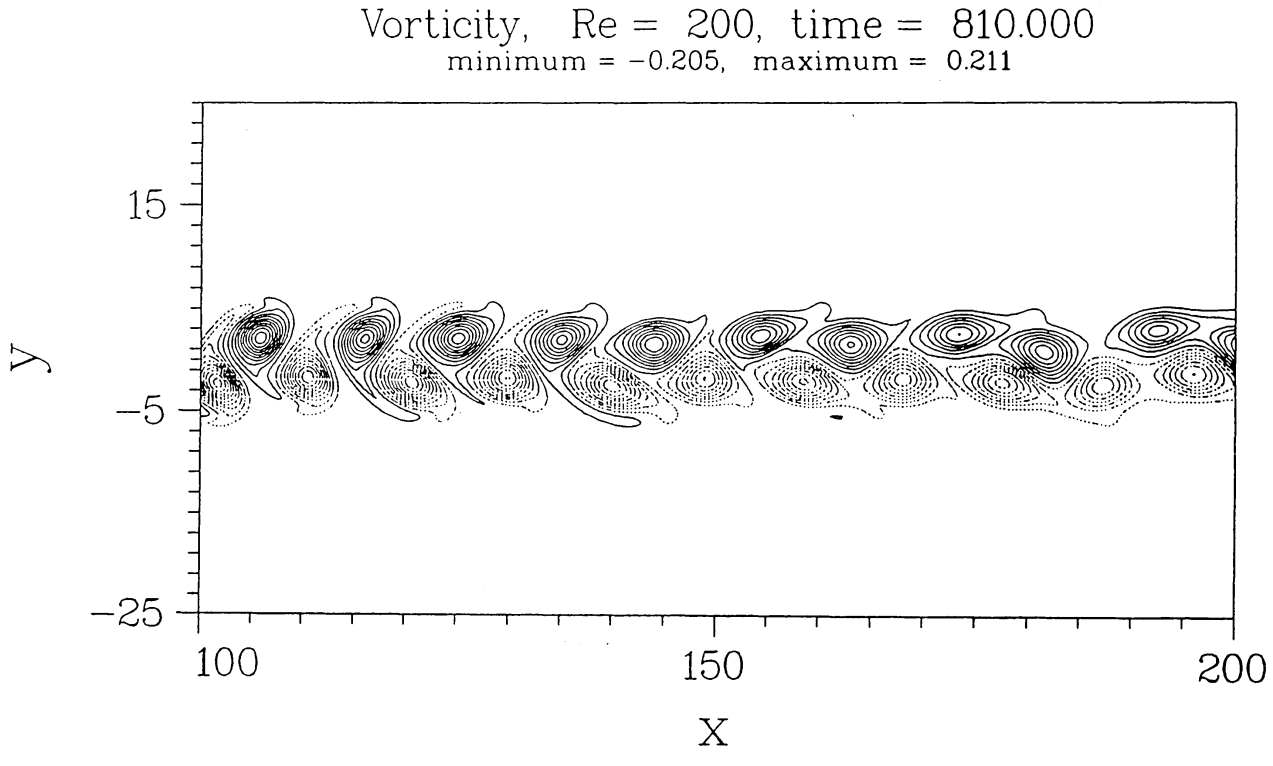
Vorticity, Re = 200, time = 810.000
minimum = −0.205, maximum = 0.211
15
−5
−25
y
100
150
200
X

Fig. 3

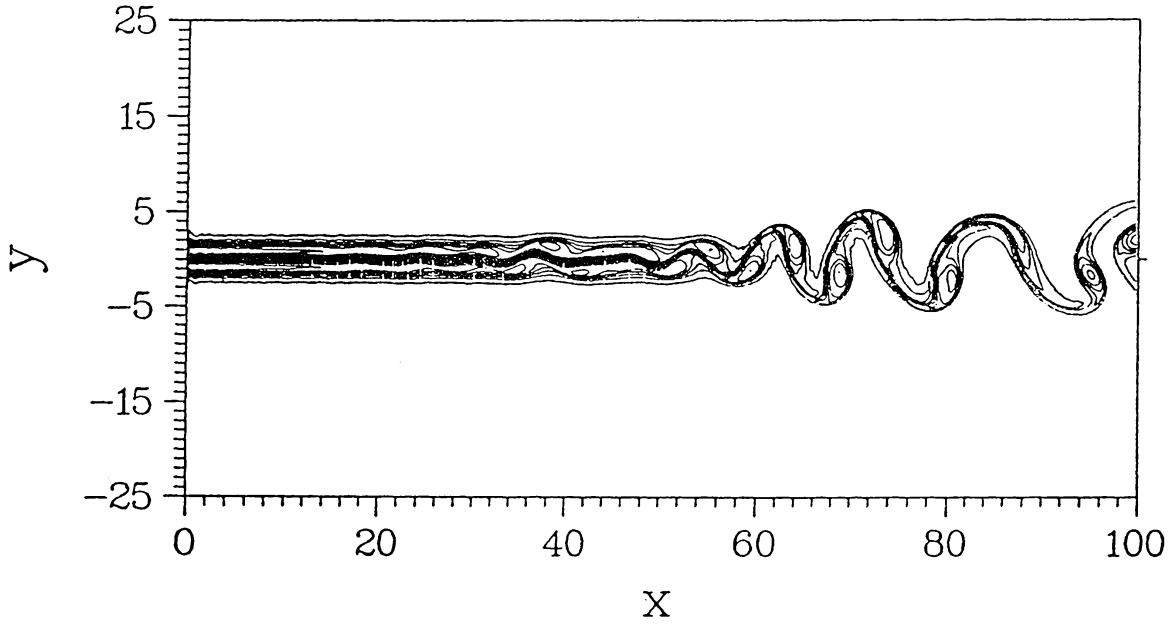
25
15
5
−5
−15
−25
y
0
20
40
60
80
100
X

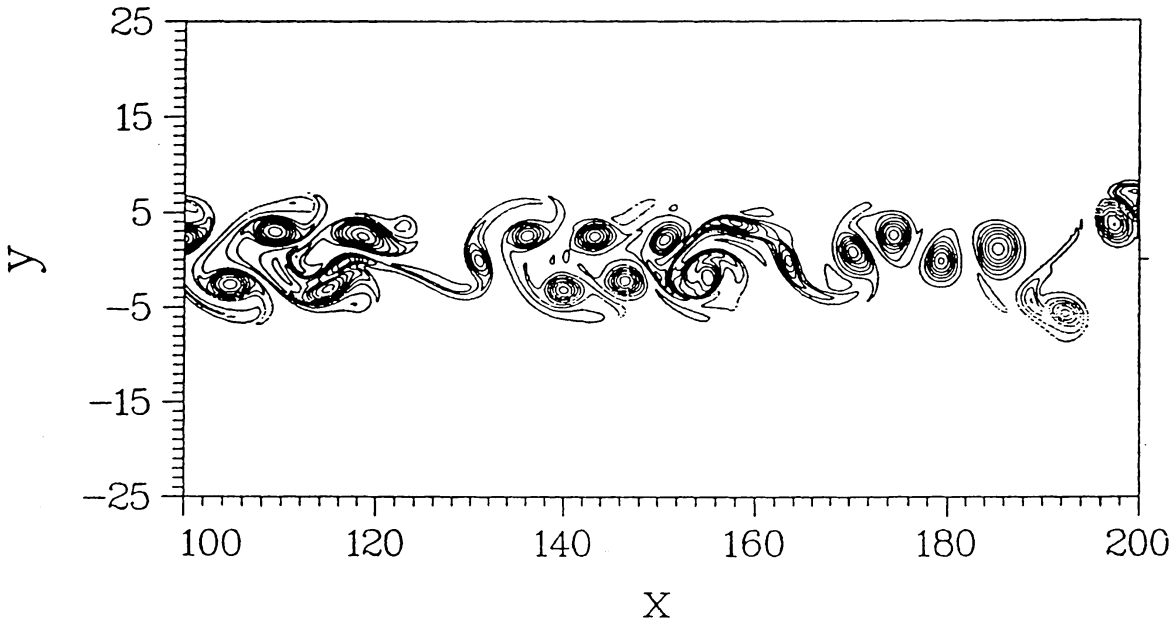
25
15
5
−5
−15
−25
y
100
120
140
160
180
200
X

Fig. 4

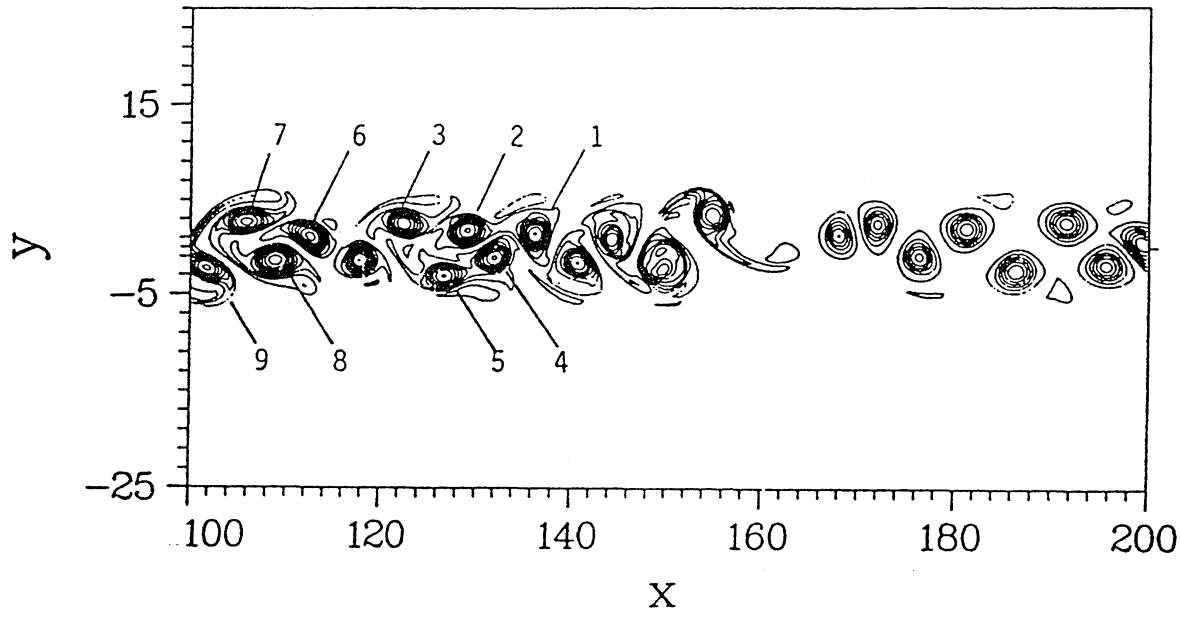
15
−5
−25
y
100
120
140
160
180
200
x
7
6
3
2
1
9
8
5
4

(a)

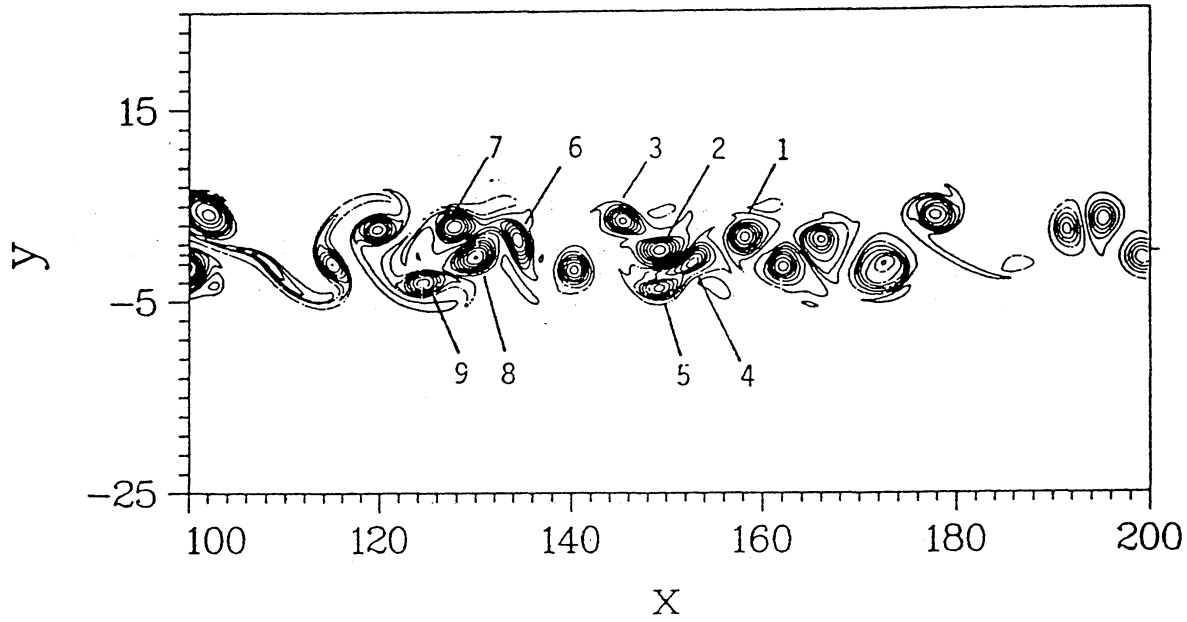
15
−5
−25
y
100
120
140
160
180
200
x
7
6
3
2
1
9
8
5
4

(b)

Fig. 5

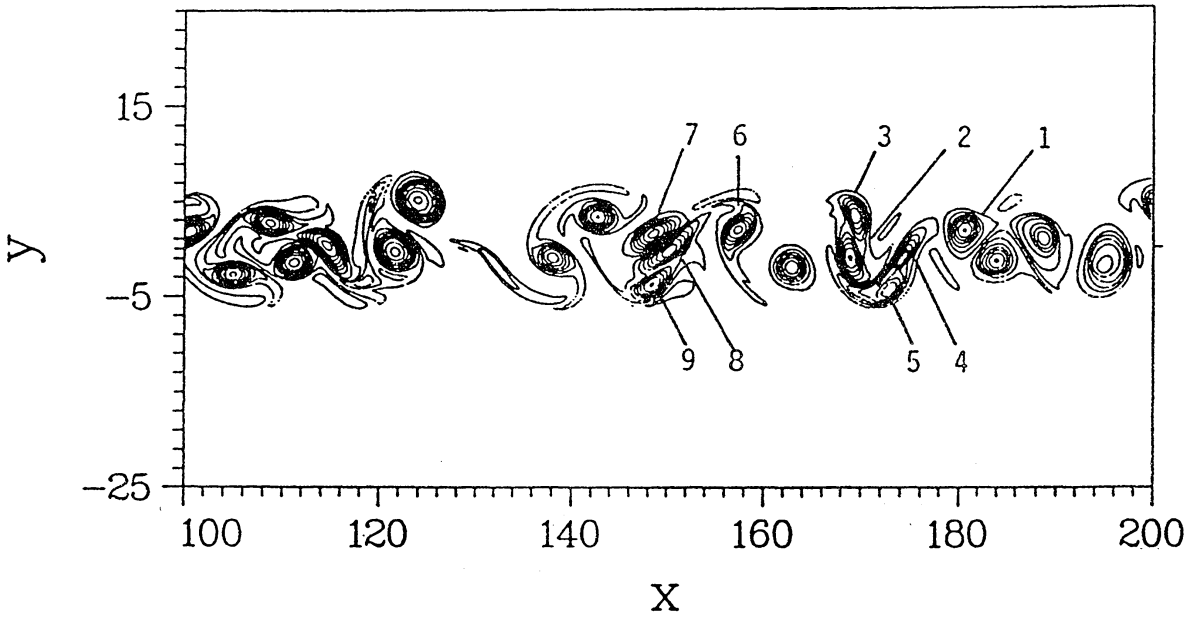
15
-5
-25
y
100
120
140
160
180
200
X
7
6
3
2
1
9
8
5
4

(c)

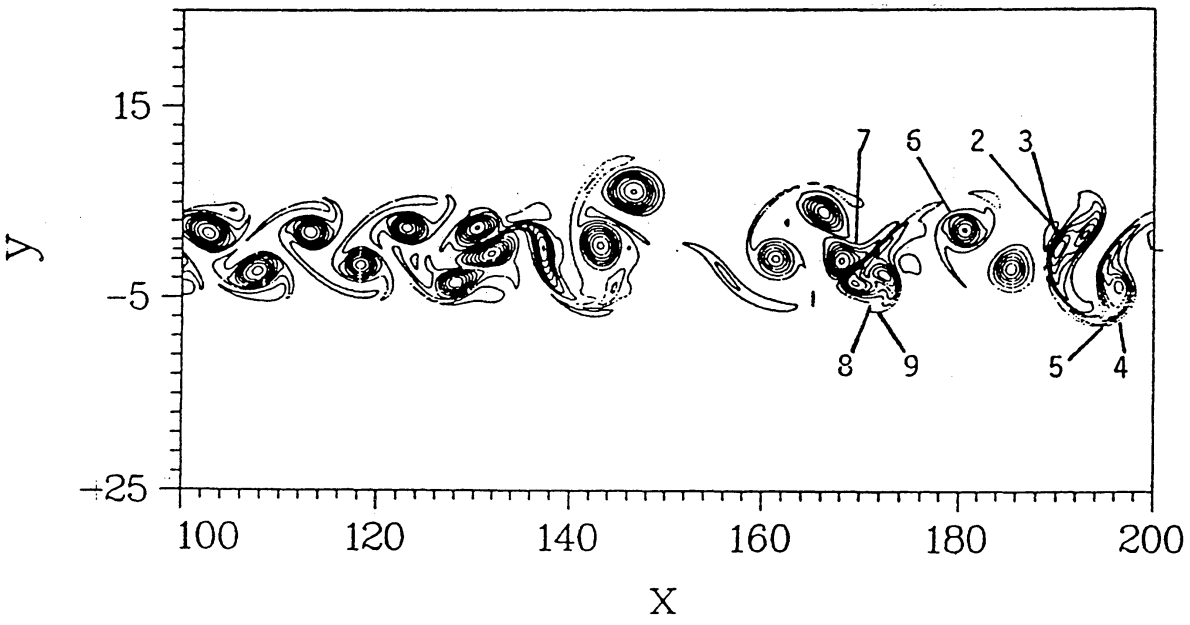
15
-5
-25
y
100
120
140
160
180
200
X
7
6
2
3
8
9
5
4

(d)

Fig. 5

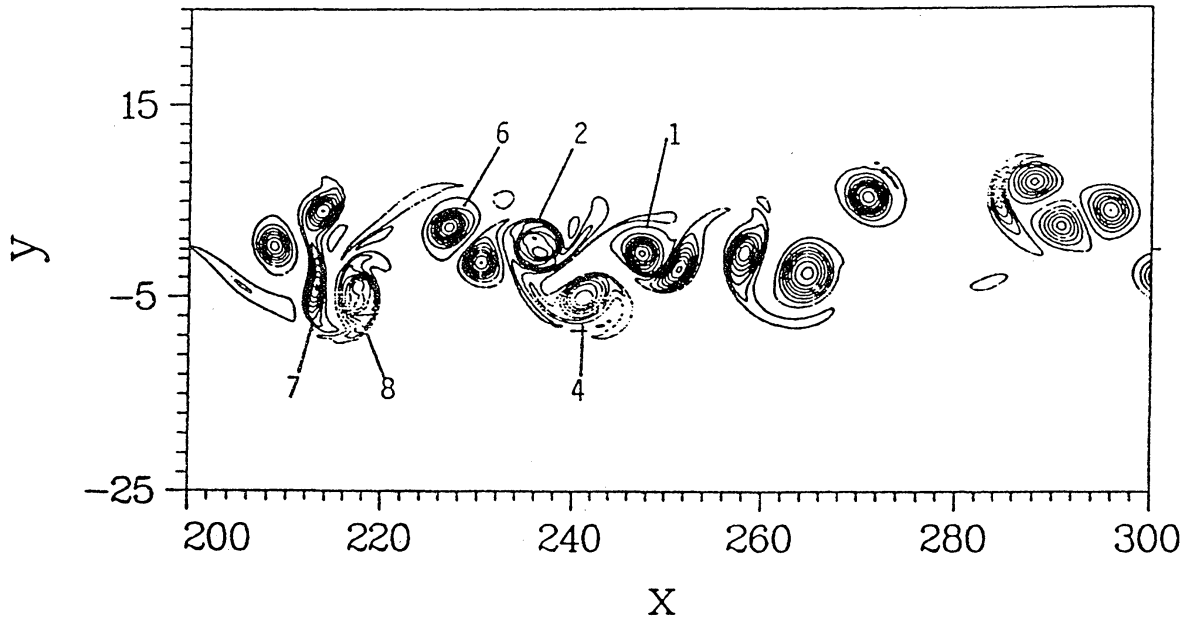
15
-5
-25
y
200
220
240
260
280
300
X
6
2
1
7
8
4

(e)

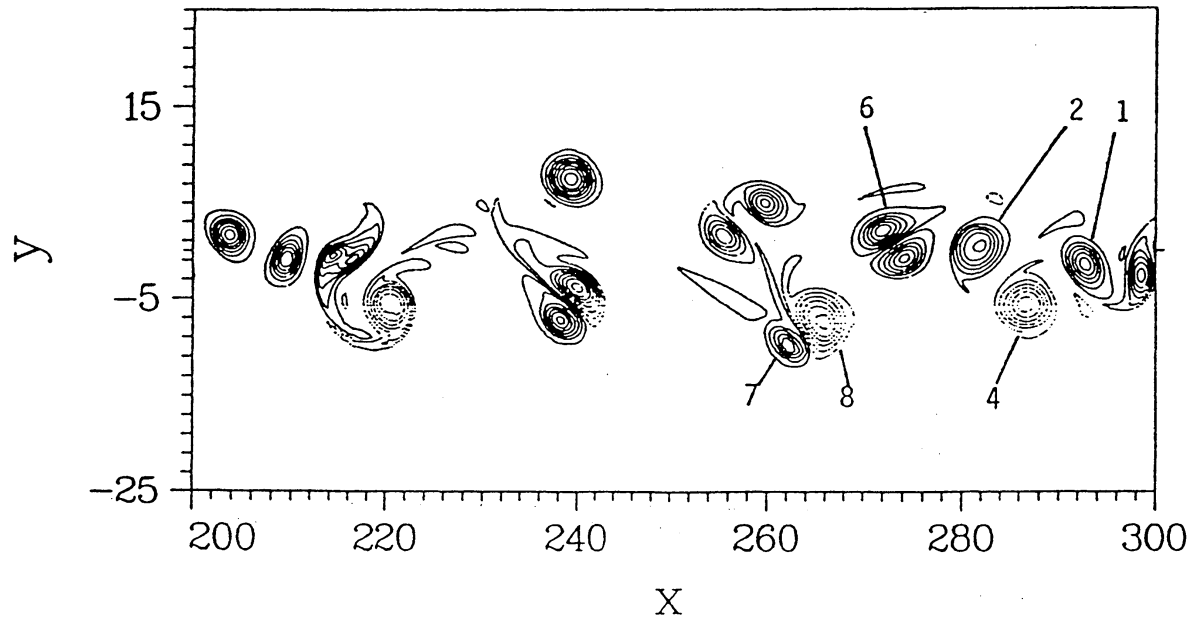
15
-5
-25
y
200
220
240
260
280
300
X
6
2
1
7
8
4

(f)

Fig. 5

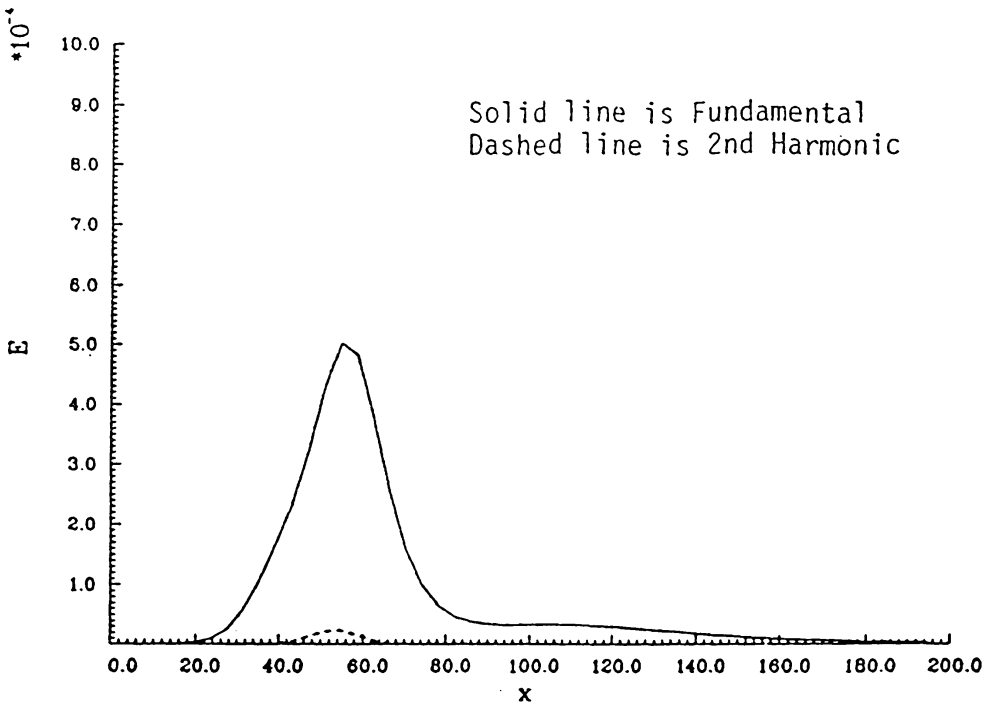
*10⁻⁴
10.0
9.0
8.0
7.0
6.0
5.0
4.0
3.0
2.0
1.0
E
Solid line is Fundamental
Dashed line is 2nd Harmonic
0.0
20.0
40.0
60.0
80.0
100.0
120.0
140.0
160.0
180.0
200.0
x

(a)

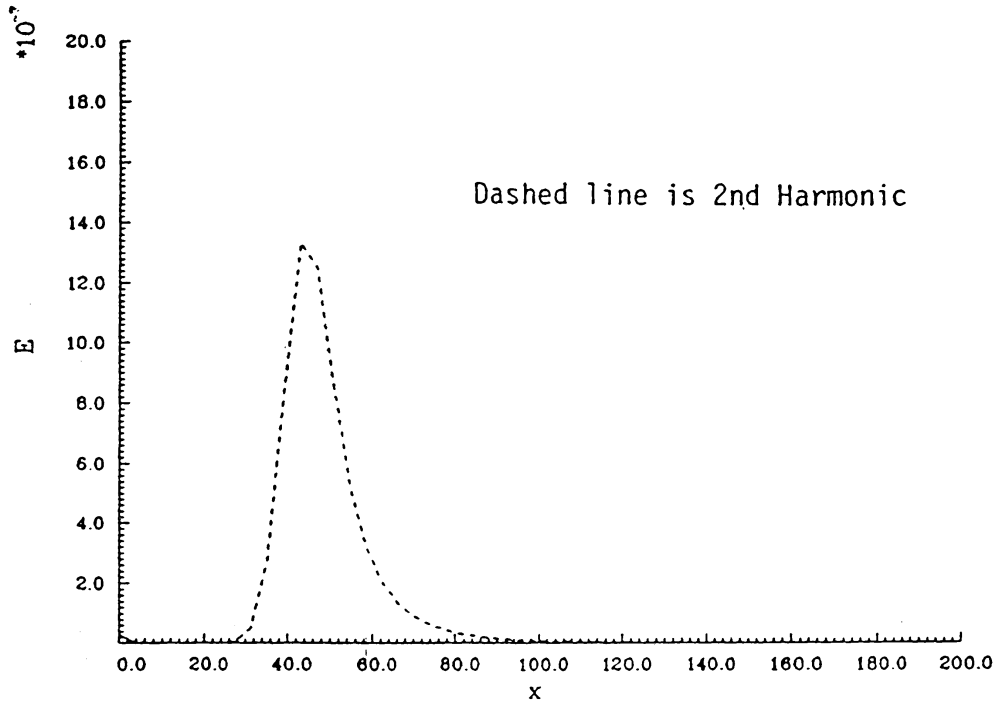
*10⁻⁵
20.0
18.0
16.0
14.0
12.0
10.0
8.0
6.0
4.0
2.0
E
Dashed line is 2nd Harmonic
0.0
20.0
40.0
60.0
80.0
100.0
120.0
140.0
160.0
180.0
200.0
x

(b)

Fig. 6

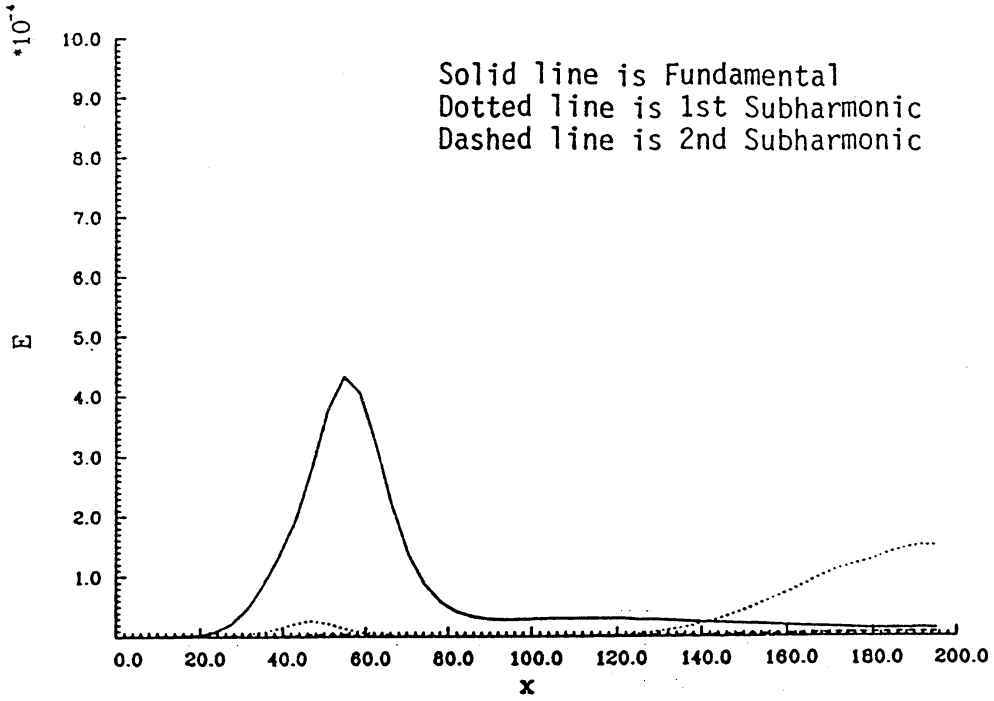
*10^-4
10.0
9.0
8.0
7.0
6.0
5.0
4.0
3.0
2.0
1.0
E
Solid line is Fundamental
Dotted line is 1st Subharmonic
Dashed line is 2nd Subharmonic
0.0
20.0
40.0
60.0
80.0
100.0
120.0
140.0
160.0
180.0
200.0
x

(a)

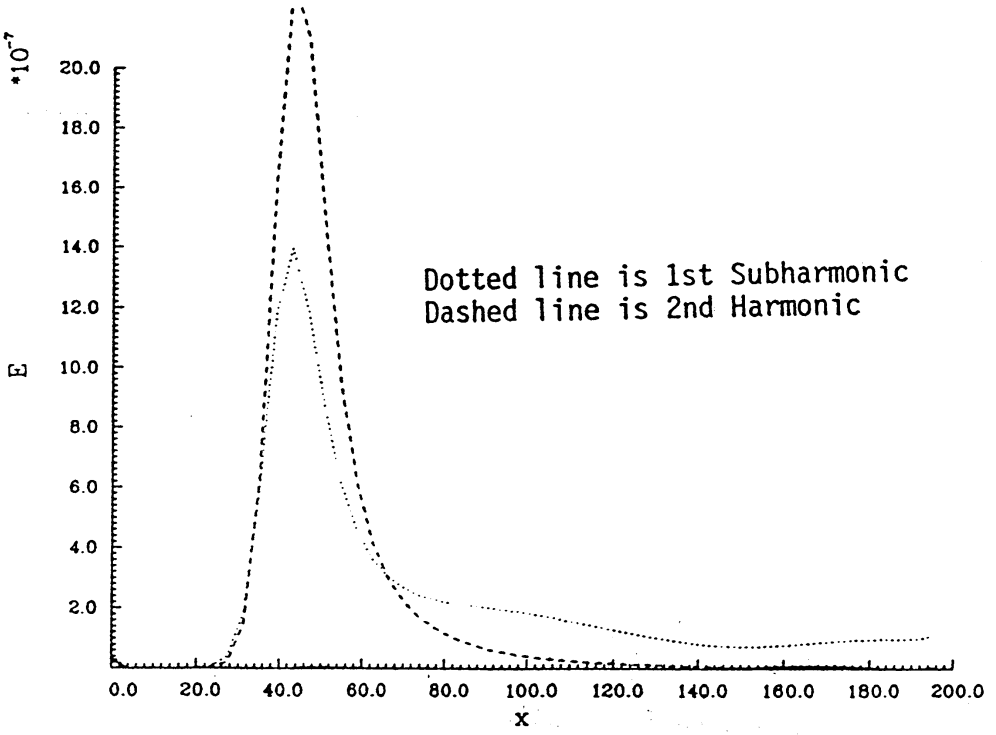
*10^-7
20.0
18.0
16.0
14.0
12.0
10.0
8.0
6.0
4.0
2.0
E
Dotted line is 1st Subharmonic
Dashed line is 2nd Harmonic
0.0
20.0
40.0
60.0
80.0
100.0
120.0
140.0
160.0
180.0
200.0
x

(b)

Fig. 7

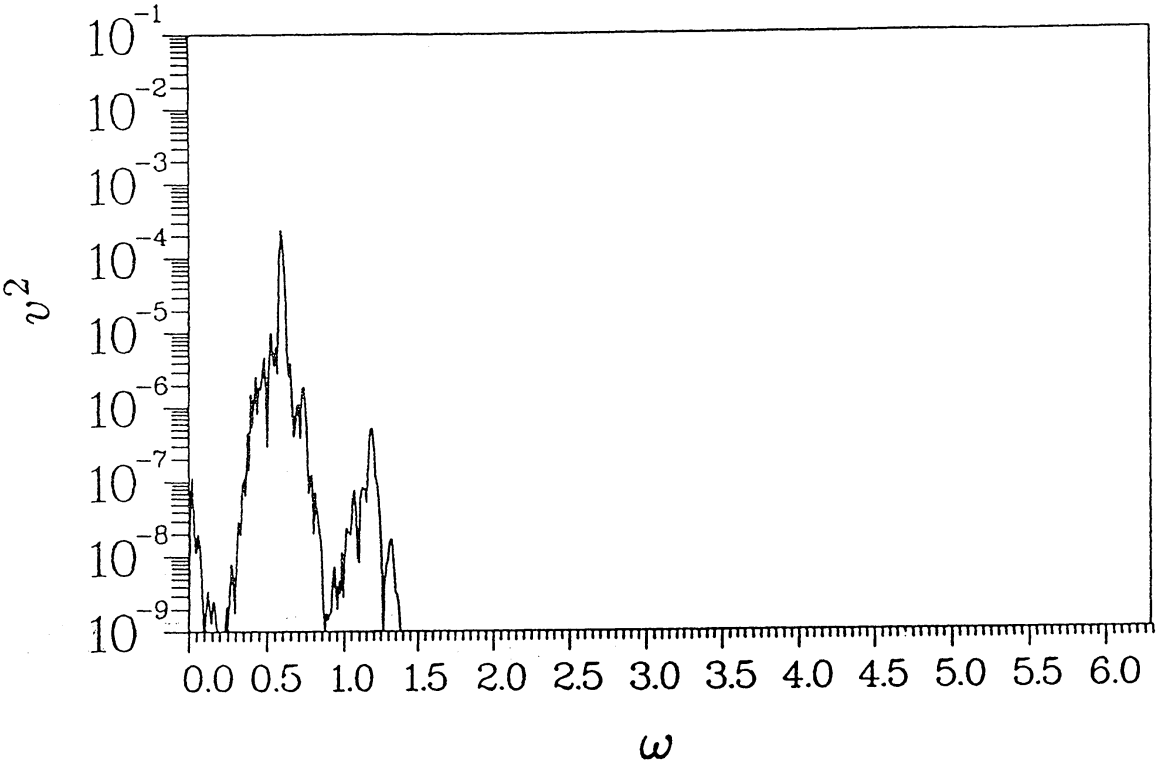
v^2
10^{-1}
10^{-2}
10^{-3}
10^{-4}
10^{-5}
10^{-6}
10^{-7}
10^{-8}
10^{-9}
0.0 0.5 1.0 1.5 2.0 2.5 3.0 3.5 4.0 4.5 5.0 5.5 6.0
ω

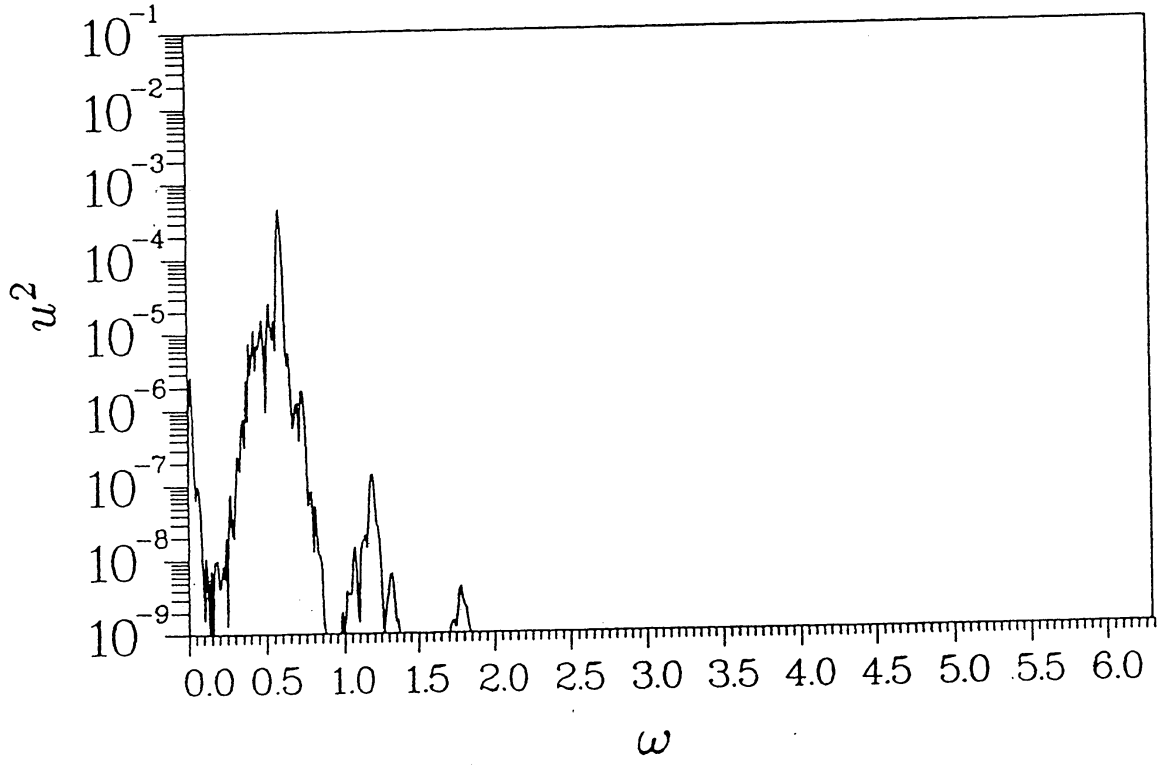
u^2
10^{-1}
10^{-2}
10^{-3}
10^{-4}
10^{-5}
10^{-6}
10^{-7}
10^{-8}
10^{-9}
0.0 0.5 1.0 1.5 2.0 2.5 3.0 3.5 4.0 4.5 5.0 5.5 6.0
ω

Fig. 8

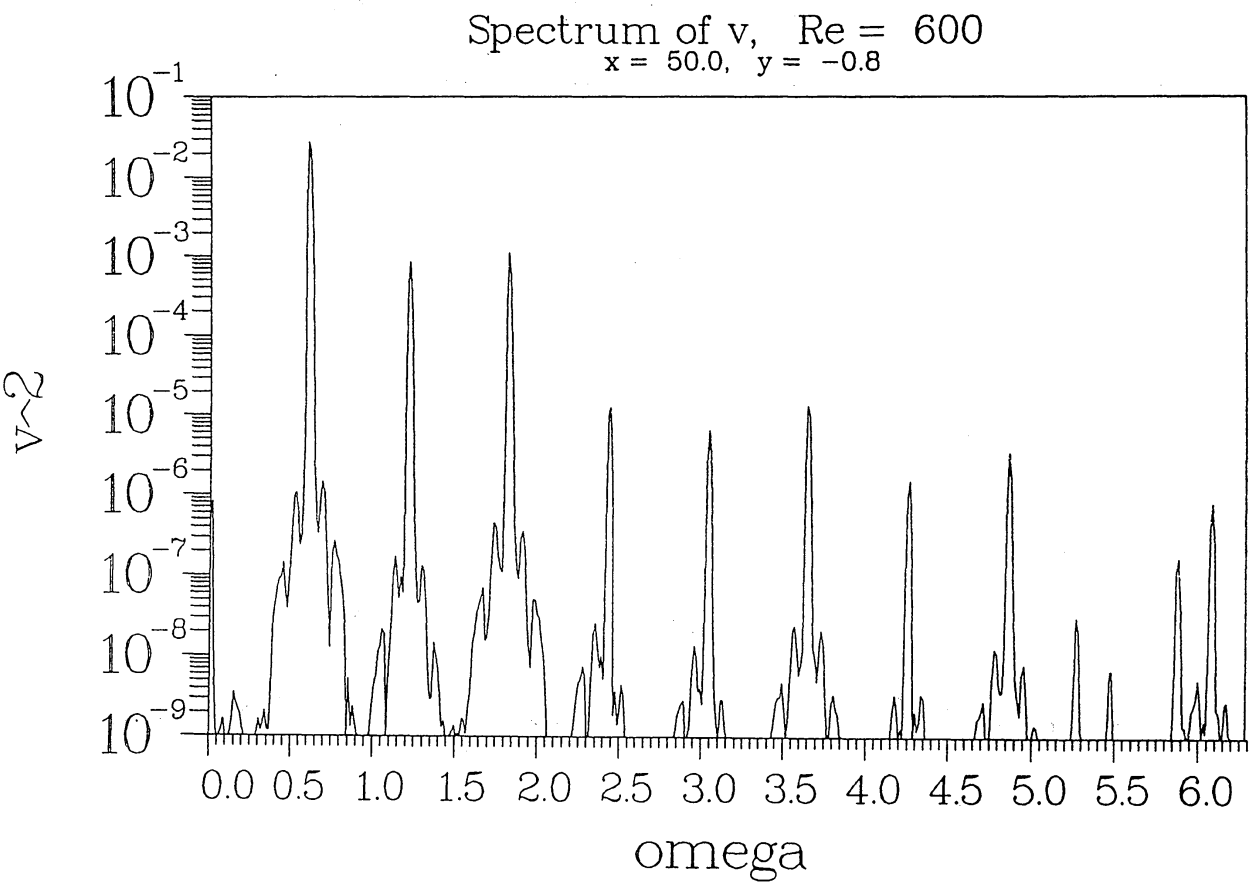
Spectrum of v, Re = 600
x = 50.0, y = -0.8
v~2
10^-1
10^-2
10^-3
10^-4
10^-5
10^-6
10^-7
10^-8
10^-9
0.0 0.5 1.0 1.5 2.0 2.5 3.0 3.5 4.0 4.5 5.0 5.5 6.0
omega

Fig. 9

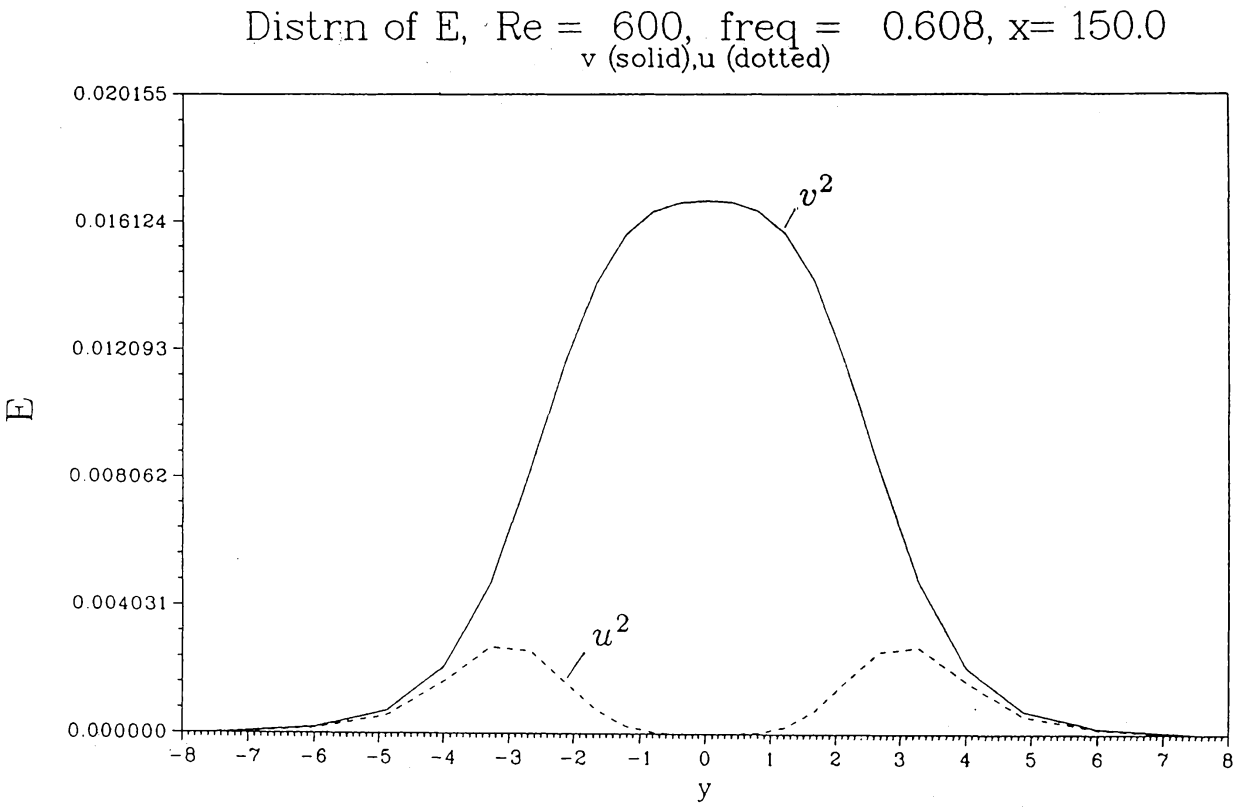
Distrn of E, Re = 600, freq = 0.608, x= 150.0
v (solid),u (dotted)
0.020155
0.016124
0.012093
0.008062
0.004031
0.000000
E
v^2
u^2
-8 -7 -6 -5 -4 -3 -2 -1 0 1 2 3 4 5 6 7 8
y

(a)

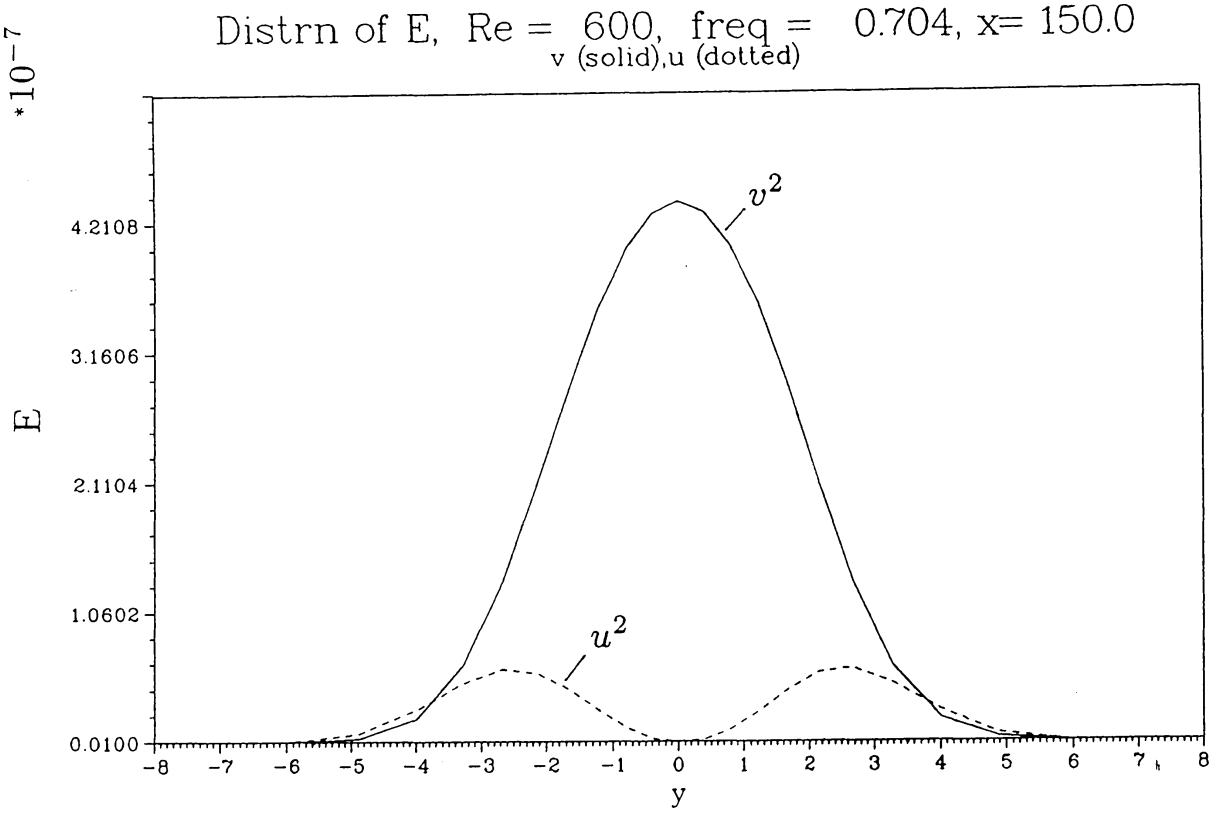
Distrn of E, Re = 600, freq = 0.704, x= 150.0
v (solid),u (dotted)
*10^-7
4.2108
3.1606
2.1104
1.0602
0.0100
E
v^2
u^2
-8 -7 -6 -5 -4 -3 -2 -1 0 1 2 3 4 5 6 7 8
y

(b)

Fig. 10

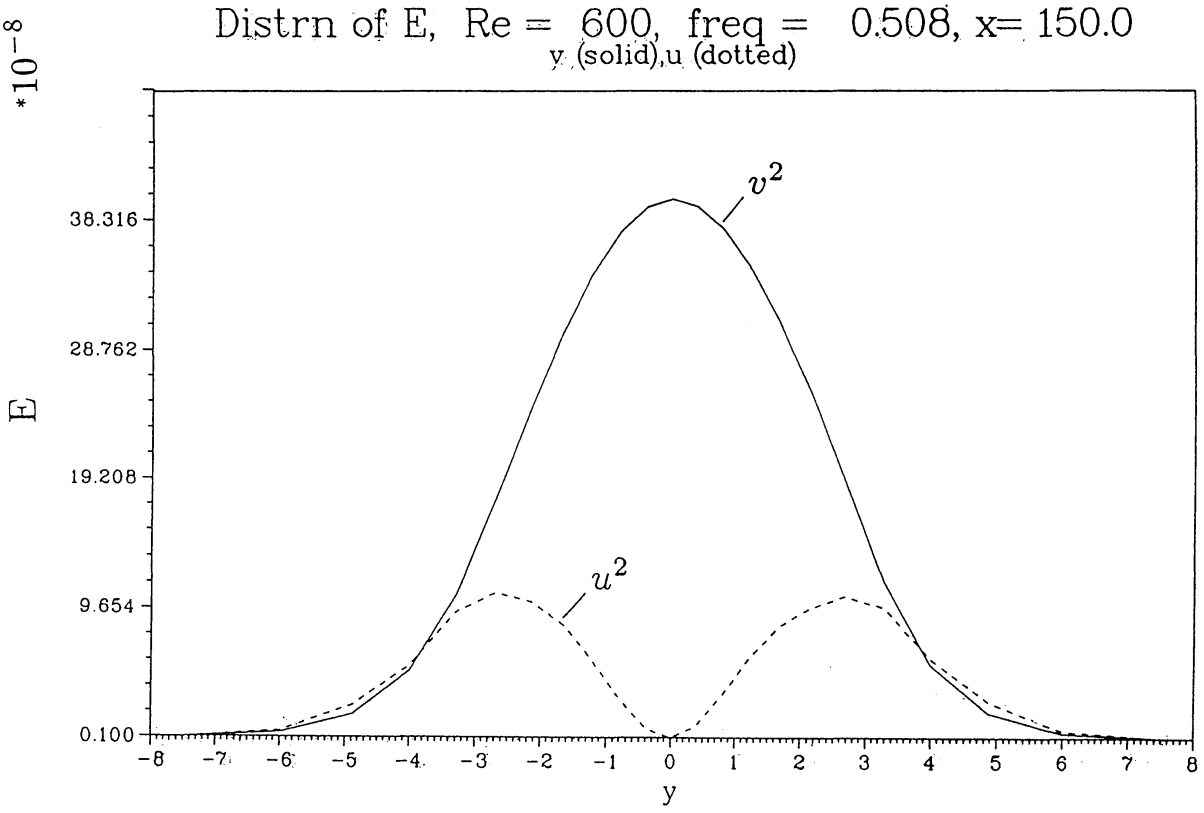
Distrn of E, Re = 600, freq = 0.508, x= 150.0
y (solid),u (dotted)
*10^-8
E
38.316
28.762
19.208
9.654
0.100
v^2
u^2
-8 -7 -6 -5 -4 -3 -2 -1 0 1 2 3 4 5 6 7 8
y

(c)

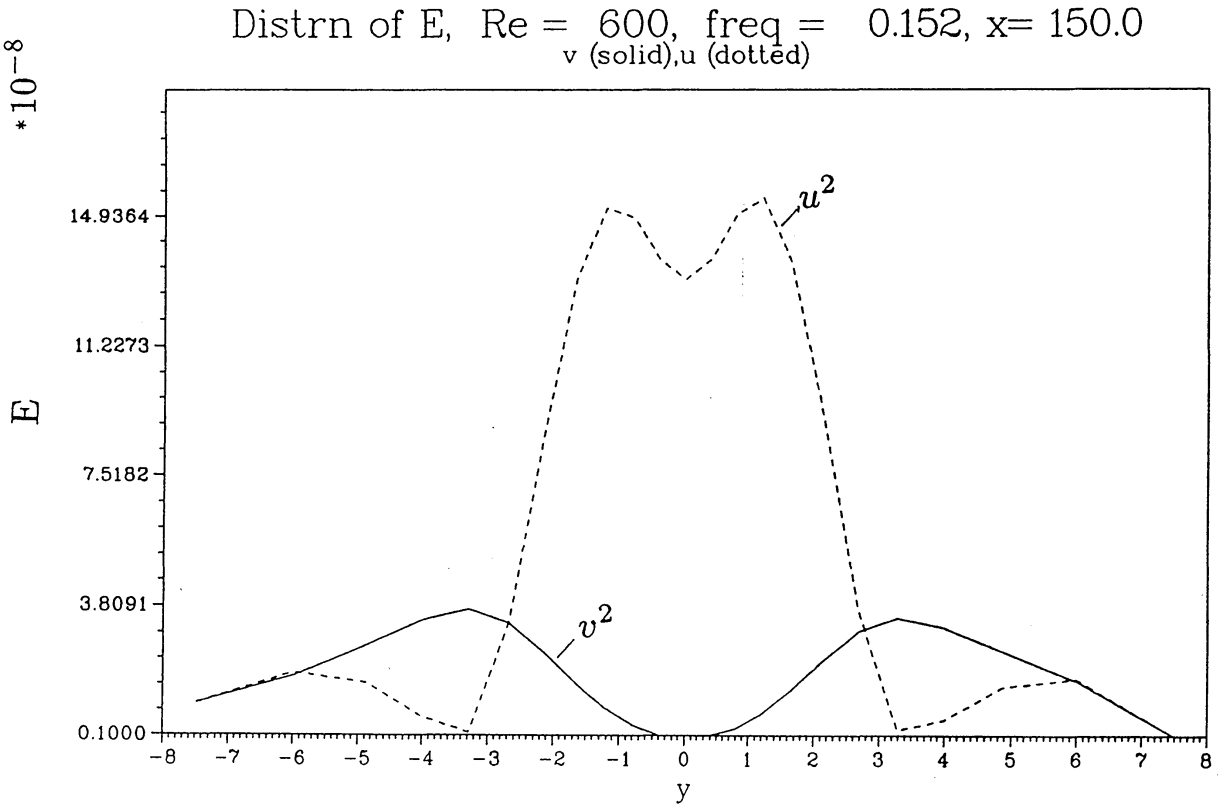
Distrn of E, Re = 600, freq = 0.152, x= 150.0
v (solid),u (dotted)
*10^-8
E
14.9364
11.2273
7.5182
3.8091
0.1000
u^2
v^2
-8 -7 -6 -5 -4 -3 -2 -1 0 1 2 3 4 5 6 7 8
y

(d)

Fig. 10

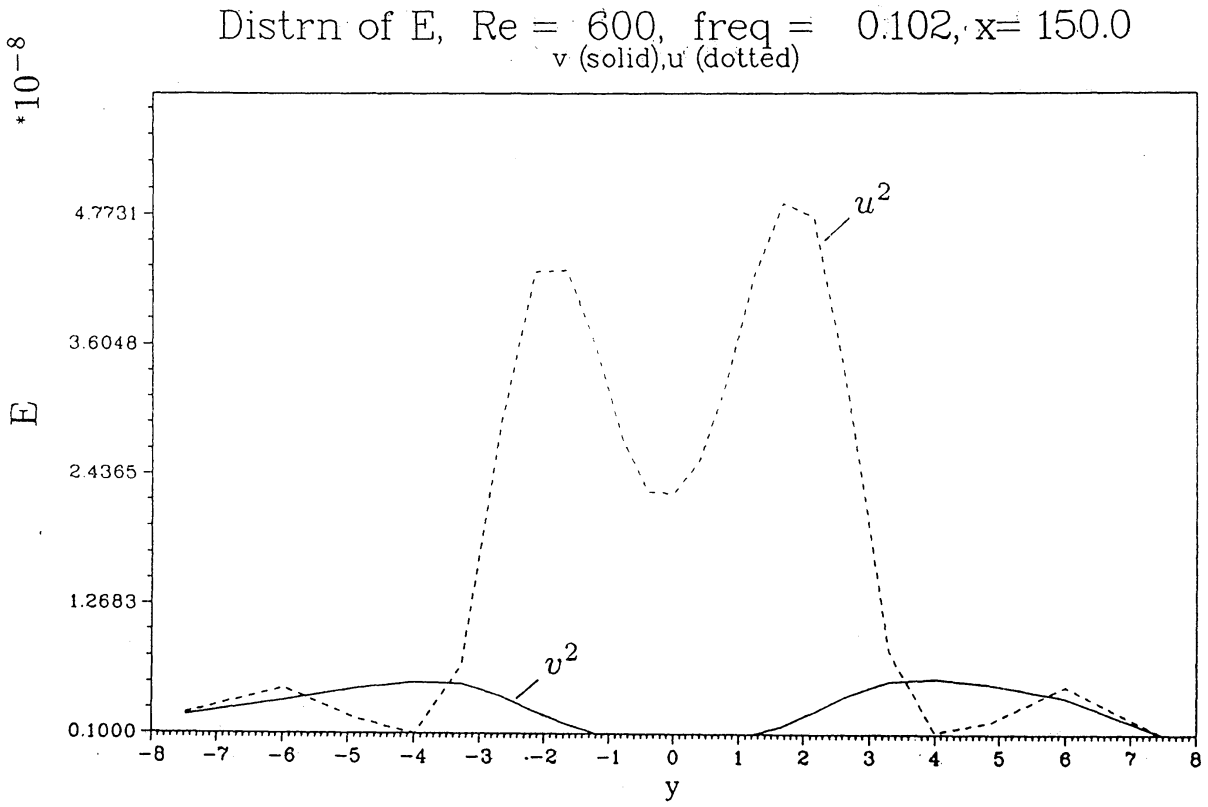
Distrn of E, Re = 600, freq = 0.102, x= 150.0
v (solid),u (dotted)
*10^-8
E
4.7731
3.6048
2.4365
1.2683
0.1000
u^2
v^2
-8 -7 -6 -5 -4 -3 -2 -1 0 1 2 3 4 5 6 7 8
y

(e)

Fig. 10

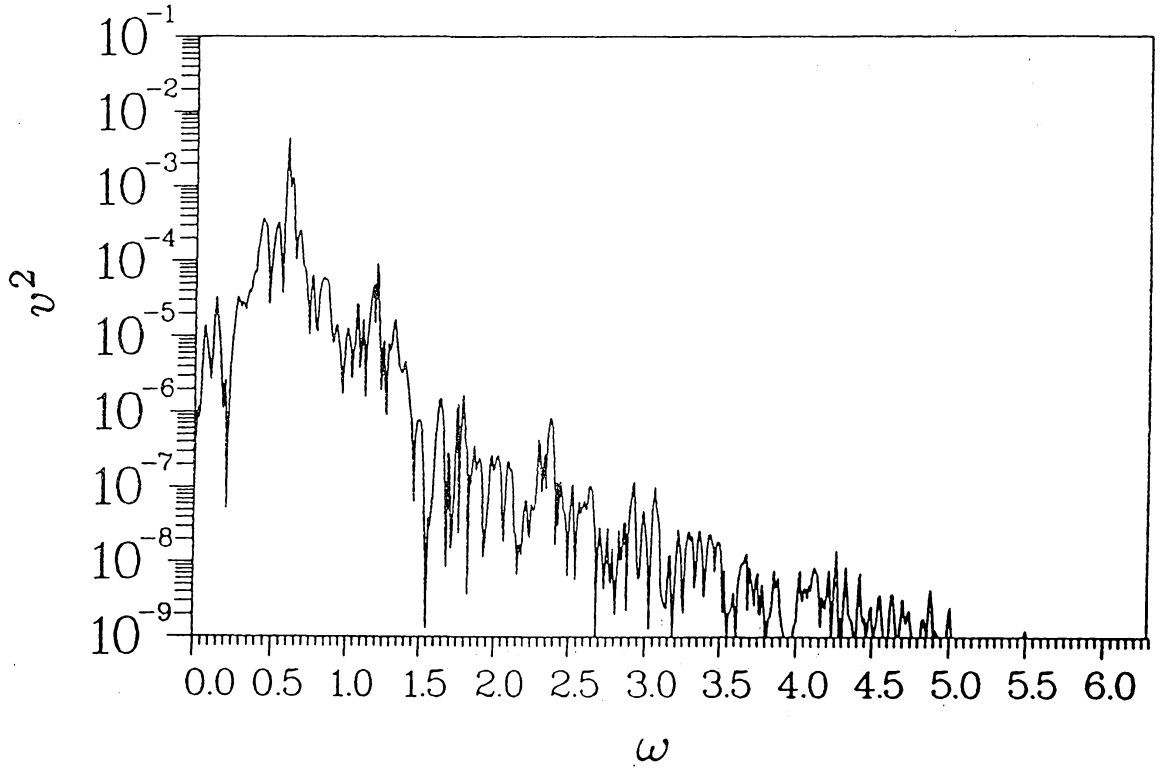
10^{-1}
10^{-2}
10^{-3}
10^{-4}
10^{-5}
10^{-6}
10^{-7}
10^{-8}
10^{-9}
v^2
0.0 0.5 1.0 1.5 2.0 2.5 3.0 3.5 4.0 4.5 5.0 5.5 6.0
ω

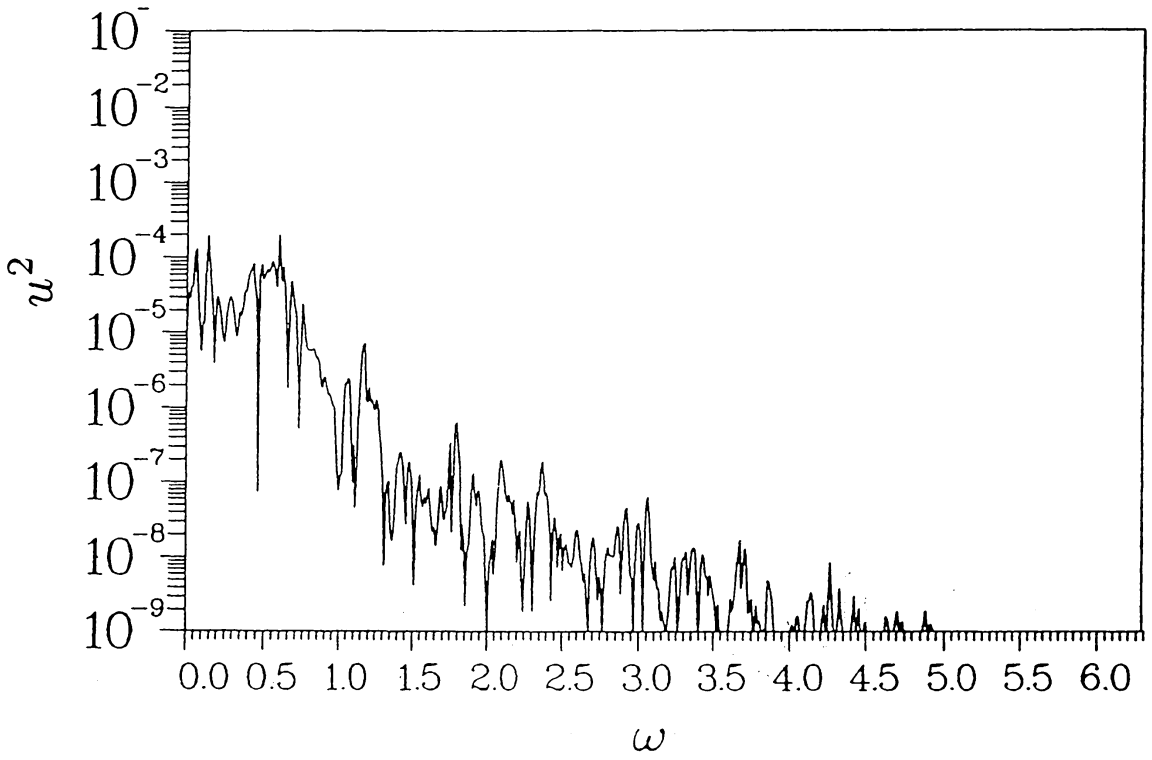
10^{-}
10^{-2}
10^{-3}
10^{-4}
10^{-5}
10^{-6}
10^{-7}
10^{-8}
10^{-9}
u^2
0.0 0.5 1.0 1.5 2.0 2.5 3.0 3.5 4.0 4.5 5.0 5.5 6.0
ω

Fig. 11

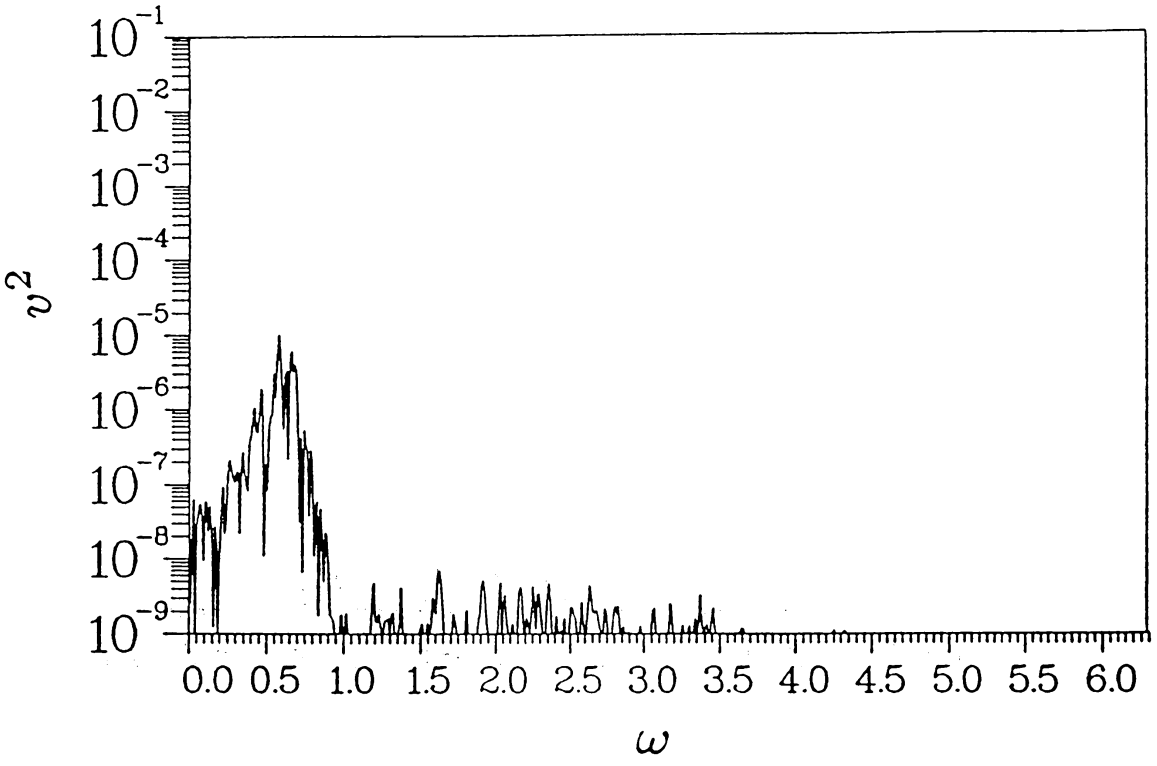
v^2
10^{-1}
10^{-2}
10^{-3}
10^{-4}
10^{-5}
10^{-6}
10^{-7}
10^{-8}
10^{-9}
0.0 0.5 1.0 1.5 2.0 2.5 3.0 3.5 4.0 4.5 5.0 5.5 6.0
ω

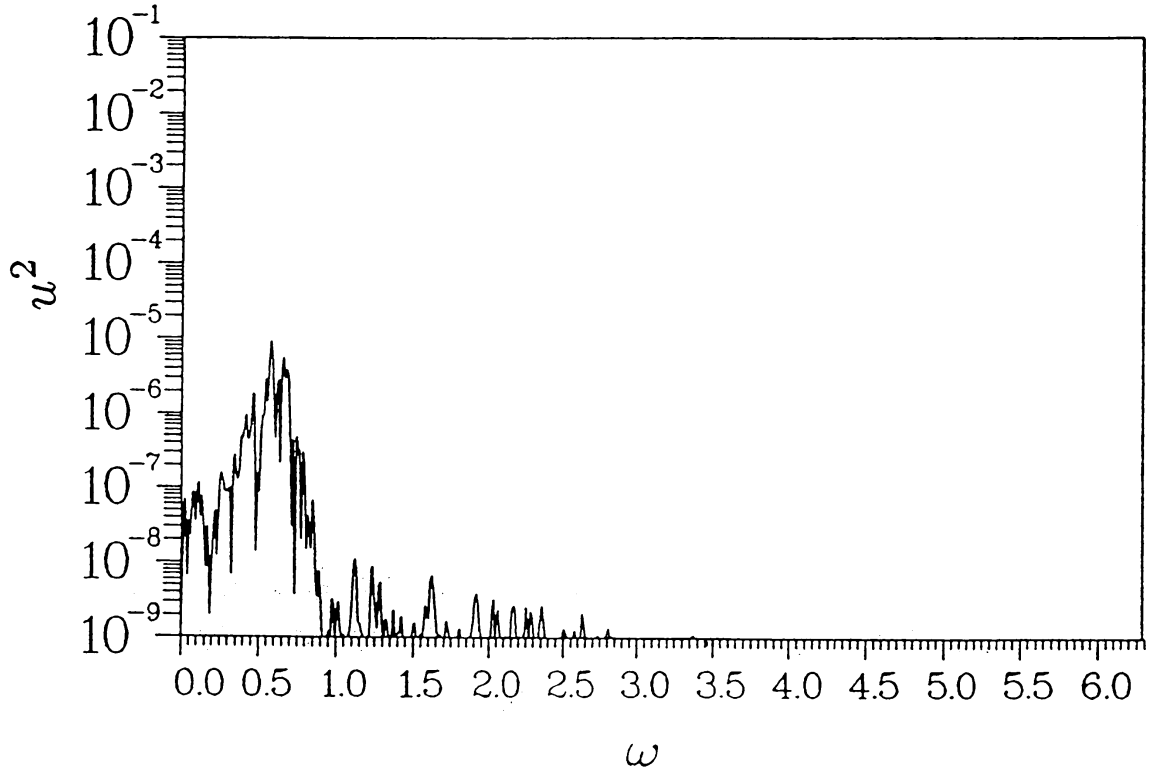
u^2
10^{-1}
10^{-2}
10^{-3}
10^{-4}
10^{-5}
10^{-6}
10^{-7}
10^{-8}
10^{-9}
0.0 0.5 1.0 1.5 2.0 2.5 3.0 3.5 4.0 4.5 5.0 5.5 6.0
ω

Fig. 12

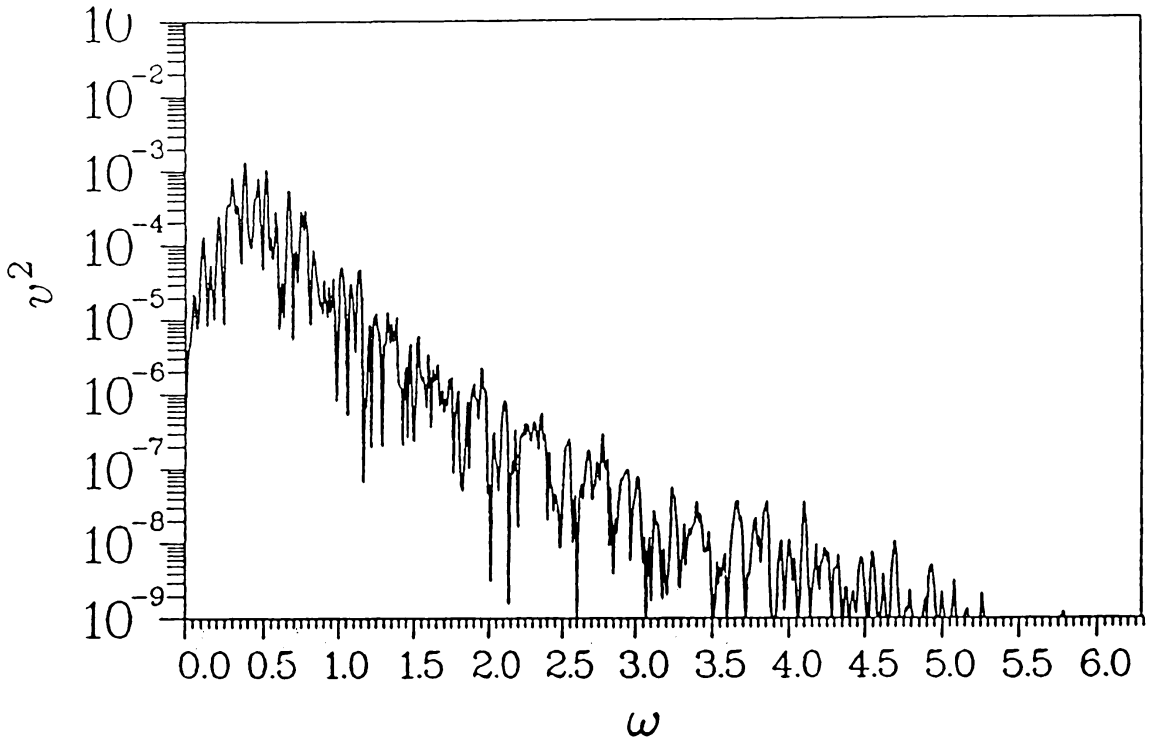
10
10^{-2}
10^{-3}
10^{-4}
10^{-5}
10^{-6}
10^{-7}
10^{-8}
10^{-9}
v^2
0.0 0.5 1.0 1.5 2.0 2.5 3.0 3.5 4.0 4.5 5.0 5.5 6.0
ω

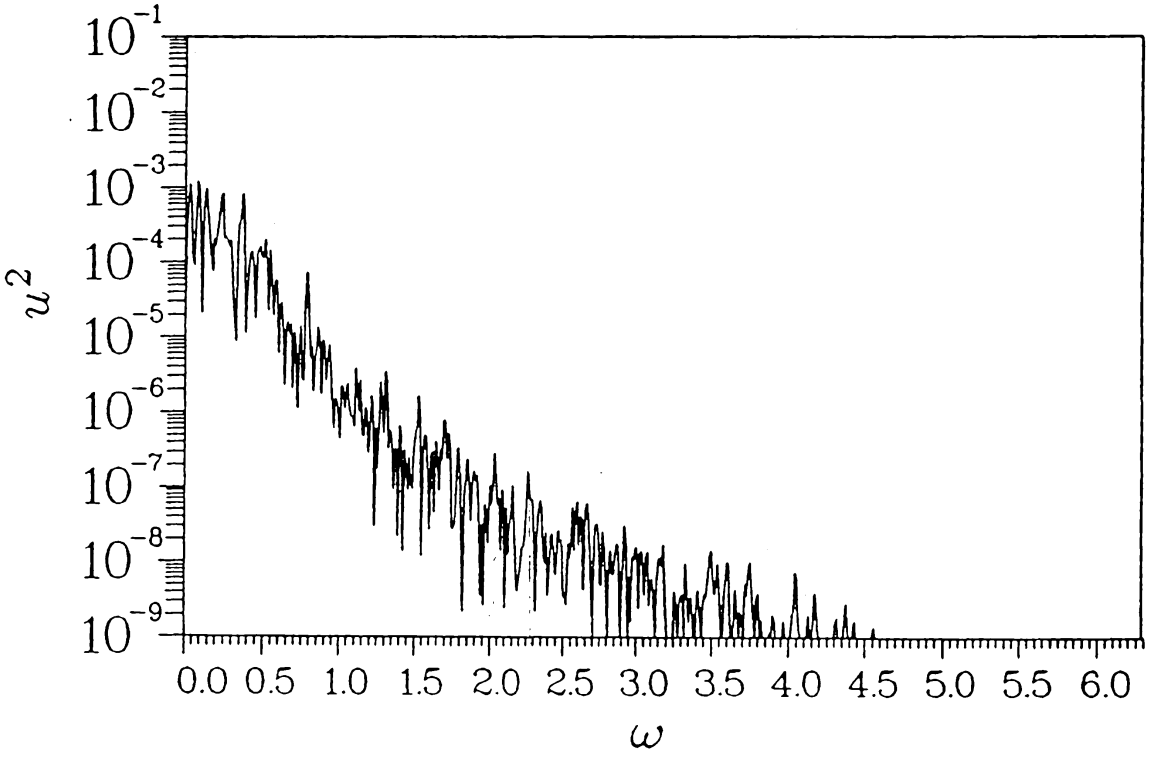
10^{-1}
10^{-2}
10^{-3}
10^{-4}
10^{-5}
10^{-6}
10^{-7}
10^{-8}
10^{-9}
u^2
0.0 0.5 1.0 1.5 2.0 2.5 3.0 3.5 4.0 4.5 5.0 5.5 6.0
ω

Fig. 13

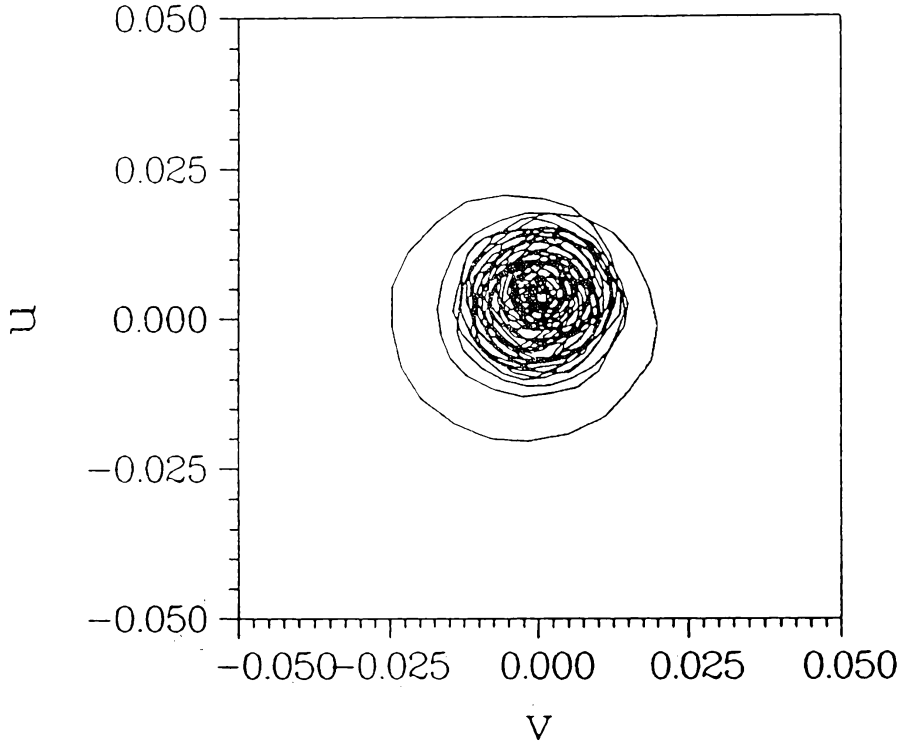
0.050
0.025
0.000
−0.025
−0.050
U
−0.050 −0.025 0.000 0.025 0.050
V

(a)

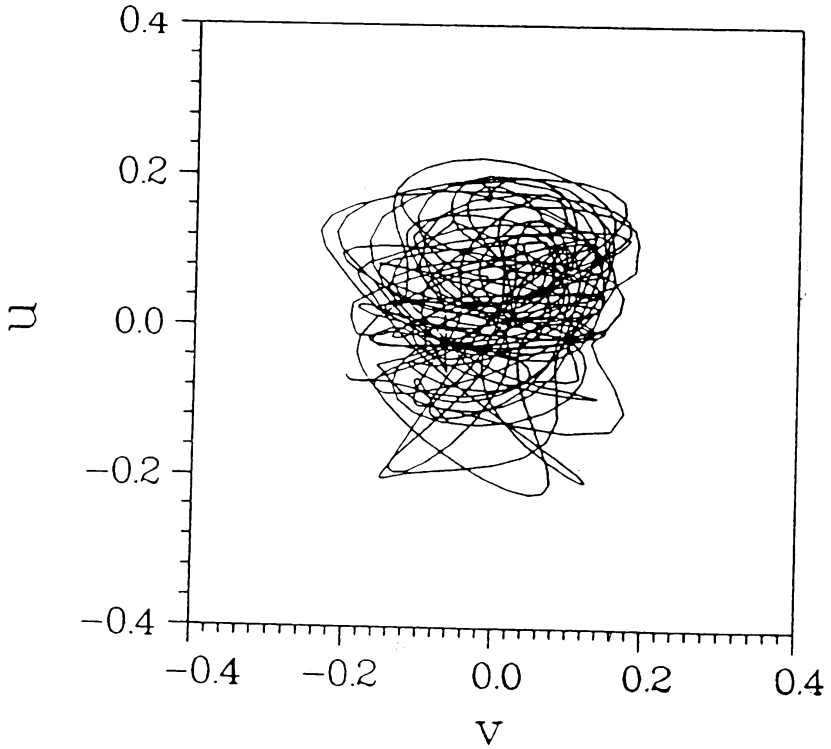
0.4
0.2
0.0
−0.2
−0.4
U
−0.4 −0.2 0.0 0.2 0.4
V

(b)

Fig. 14

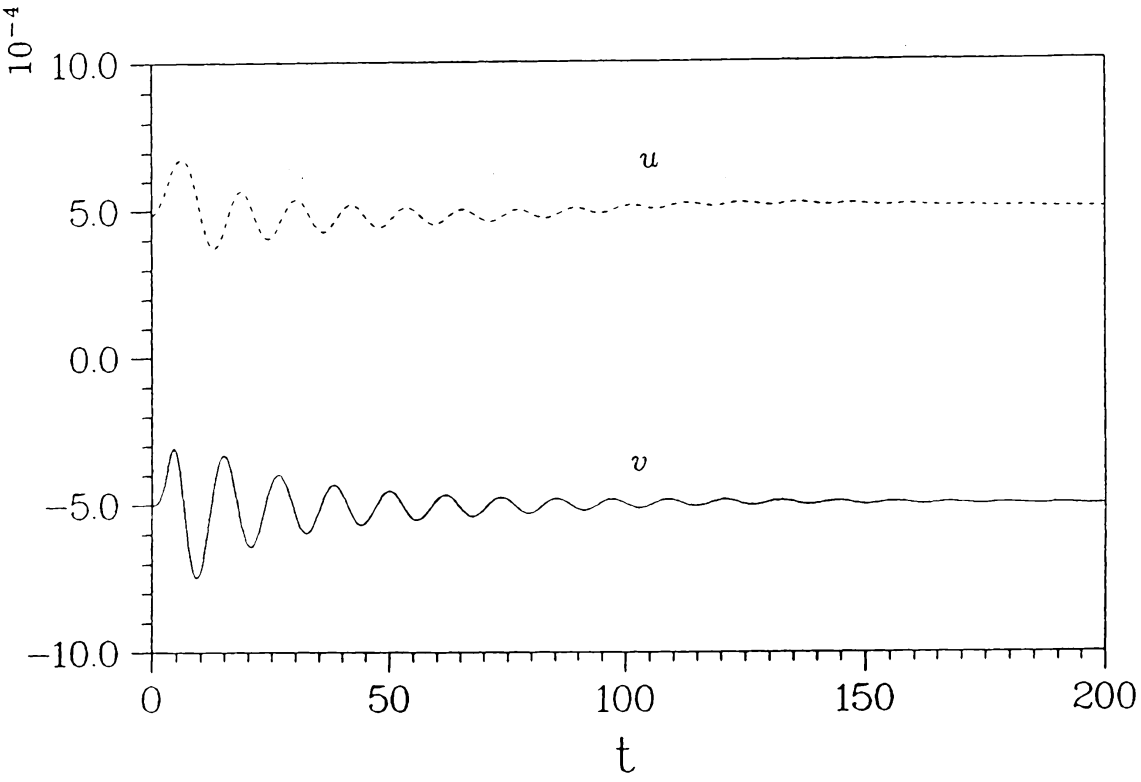
10^{-4}
10.0
5.0
0.0
−5.0
−10.0
u
v
0
50
100
150
200
t

(a)

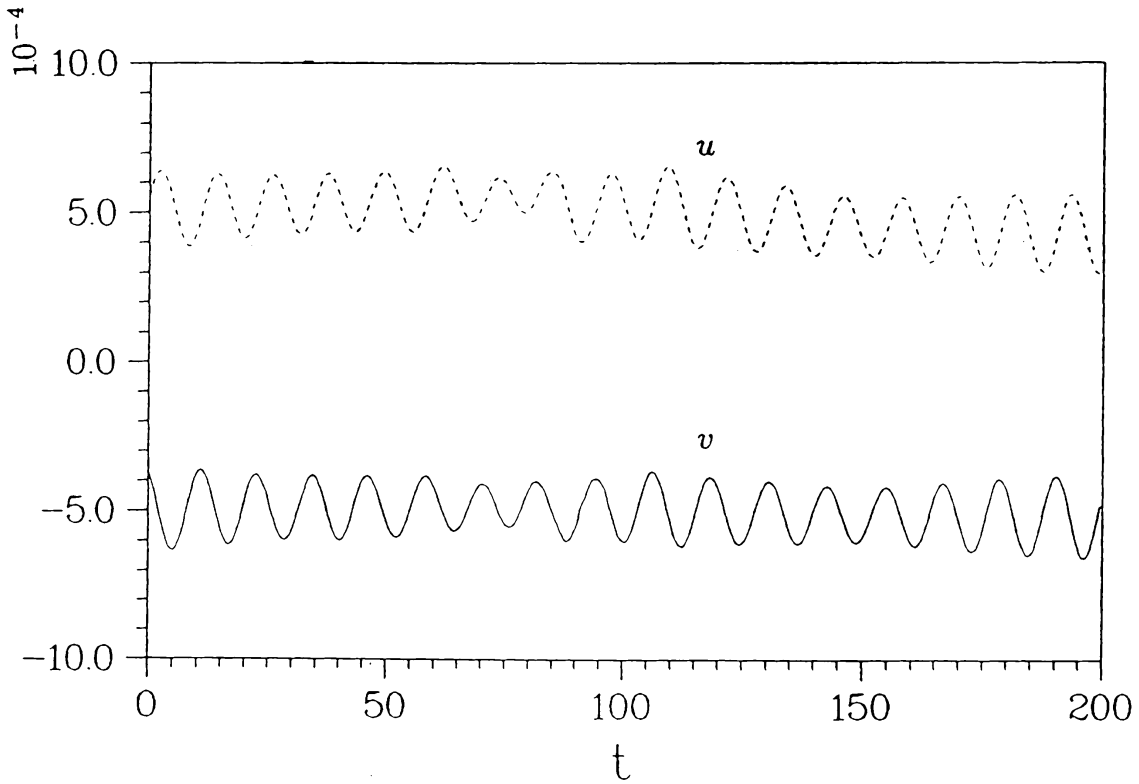
10^{-4}
10.0
5.0
0.0
−5.0
−10.0
u
v
0
50
100
150
200
t

(b)

Fig. 15